CFL-FREE NUMERICAL SCHEMES FOR THE TWO-FLUID MODEL

STEINAR EVJE[A,C] AND TORE FLATTEN[B]

Abstract. The main purpose of this paper is to construct an implicit numerical scheme for a two-phase flow model, allowing for violation of the CFL-criterion for all waves. Based on the *Mixture Flux* (MF) approach developed in [12] we propose both a *Weakly Implicit* MF (WIMF) scheme, similar to the one studied in [11], and a *Strongly Implicit* MF (SIMF) scheme. The WIMF scheme is stable for a weak CFL condition which relates time steps to the fluid velocity whereas the SIMF scheme is unconditionally stable, at least for a moving contact discontinuity. Both schemes apply AUSM (advection upstream splitting methods) type of convective fluxes.

The SIMF scheme is obtained by enforcing a stronger implicit coupling between the mass equations than the one used for the WIMF scheme. The resulting scheme allows for sequential updating of the momentum and mass variables on a nonstaggered grid by solving two sparse linear systems. The scheme is conservative in all convective fluxes and consistency between the mass variables and pressure is formally maintained. We present numerical simulations indicating that the CFL-free scheme maintains the good accuracy and stability properties of the WIMF scheme as well as an explicit Roe scheme for small time steps.

Moreover, we demonstrate that the WIMF scheme is able to give an *exact* resolution of a *moving* contact discontinuity. Explicit schemes cannot possess this property since it closely hang on the fact that the time step can be related to the fluid velocity. This feature of the WIMF scheme explains why it is very accurate for calculation of unsteady two-phase flow phenomena, as was also observed in [11]. The SIMF scheme does not possess the "exact resolution" property of WIMF, however, the ability to take larger time steps can be exploited so that more efficient calculations can be made when accurate resolution of sharp fronts is not essential, e.g. to calculate steady state solutions.

subject classification. 76T10, 76N10, 65M12, 35L65

key words. two-phase flow, two-fluid model, hyperbolic system of conservation laws, flux splitting, implicit scheme

1. Introduction

We consider in this paper the *two-fluid model* governing two-phase flow of gas and liquid in a pipeline. Here each phase is treated separately in terms of two sets of conservation equations, averaged in space to yield a one-dimensional model. The interaction terms between the two phases appear in the basic equations as transfer terms across the interfaces (source terms).

More precisely, the basic form of the model can be written on the following vector form:

$$\partial_t \begin{pmatrix} \rho_{\rm g}\alpha_{\rm g} \\ \rho_{\rm l}\alpha_{\rm l} \\ \rho_{\rm g}\alpha_{\rm g}v_{\rm g} \\ \rho_{\rm l}\alpha_{\rm l}v_{\rm l} \end{pmatrix} + \partial_x \begin{pmatrix} \rho_{\rm g}\alpha_{\rm g}v_{\rm g} \\ \rho_{\rm l}\alpha_{\rm l}v_{\rm l} \\ \rho_{\rm g}\alpha_{\rm g}v_{\rm g}^2 + \alpha_{\rm g}p \\ \rho_{\rm l}\alpha_{\rm l}v_{\rm l}^2 + \alpha_{\rm l}p \end{pmatrix} = \begin{pmatrix} 0 \\ 0 \\ p\partial_x\alpha_{\rm g} + \tau_{\rm g} \\ p\partial_x\alpha_{\rm l} + \tau_{\rm l} \end{pmatrix} + \begin{pmatrix} 0 \\ 0 \\ Q_{\rm g} + M_{\rm g}^{\rm D} \\ Q_{\rm l} + M_{\rm l}^{\rm D} \end{pmatrix}. \tag{1}$$

Here α_k is the volume fraction of phase k with $\alpha_{\rm l} + \alpha_{\rm g} = 1$, ρ_k and v_k denote the density and fluid velocities of phase k, and p is the pressure common to both phases. Moreover, τ_k represents the interfacial forces which contain differential terms (hence, is relevant for the hyperbolicity of the

Date: August 18, 2003.

[A]RF-Rogaland Research, P. O. Box 8046, N-4068 Stavanger, Norway.

[B]Department of Energy and Process Engineering, Norwegian University of Science and Technology, Kolbjørn Hejes vei 1B, N-7491, Trondheim, Norway.

Email: steinar.evje@rf.no, tore.flatten@maskin.ntnu.no.

[C]Corresponding author.

model) and satisfy $\tau_{\rm g} + \tau_{\rm l} = 0$. $M_k^{\rm D}$ represents interfacial drag force with $M_{\rm g}^{\rm D} + M_{\rm l}^{\rm D} = 0$ whereas Q_k represent source terms due to gravity, friction, etc.

The majority of computer software for such two-fluid simulations are based on implicit time integration, allowing for violation of the CFL criterion

$$\frac{\Delta x}{\Delta t} \geq |\lambda_{\rm max}| \tag{2}$$

where $\lambda_{\rm max}$ is the largest eigenvalue for the system. Examples include the CATHARE code [2] developed for the nuclear industry, as well as OLGA [3] and PeTra [13] aimed towards the petroleum industry.

Following [11], we classify implicit schemes as follows:

- *Weakly implicit.* The original CFL criterion (2) may be broken for sonic waves, but a weaker CFL criterion for volume fraction waves still applies

$$\frac{\Delta x}{\Delta t} \geq |\lambda_{\rm max}^{\rm v}|, \tag{3}$$

  where $\lambda_{\rm max}^{\rm v}$ is the largest of the two eigenvalues corresponding to volume fraction waves.
- *Strongly implicit.* No CFL-like stability criterion applies and the equations may in principle be integrated with arbitrary timestep. In practice, a stability criterion applies related to the inherent stiffness of the equation system. However, by freeing themselves from CFL considerations, strongly implicit schemes may allow for larger timesteps (and hence potentially more efficient computation) than weakly implicit schemes.

To build a fully discrete numerical scheme we need a basis splitting technique for the discretization of the pressure and convective fluxes at the cell interfaces. For one-phase flow, the AUSM (Advection Upstream Splitting Method) and its derivatives [16, 15, 27, 7] have proved highly successfull. These ideas have been extended to two-phase flow models by Niu [17, 18], Edwards et al [6] and Evje and Fjelde [8, 9].

For the two-fluid model we will be concerned with here, Paillére et al [19] studied an extension of the AUSM$^+$ scheme of Liou [15]. Evje and Flatten [10] investigated an extension of the AUSMD scheme of Wada and Liou [27]. Common to both these approaches is an inherent accuracy comparable to approximate Riemann solvers, achieved by a computationally cheap algorithm. However, spurious oscillations and overshoots are observed near discontinuities.

This problem was to a large extent solved by taking the coupling between the mass equations into account [12]. This approach, denoted as the *Mixture Flux* (MF) methods, involves a rough splitting of the mass fluxes into a fast-moving and a slow-moving component dependent of properties of the mixture. In a previous work [11], we developed a weakly implicit scheme, termed *WIMF-AUSMD*, based on the MF approach combined with the use of AUSMD convective fluxes similar to those applied in [10].

The purpose of the present work is to elaborate further on the class of MF schemes for the two-fluid model. The MF methods are first presented in a semidiscrete setting, similar to the one introduced in [11]. Particularly, the MF methods are constructed so that they satisfy the following "good" properties: (i) The numerical mass fluxes reduce to upwind type of fluxes for a linear contact discontinuity similar to those produced by an exact riemann solver; (ii) Abgrall's principle is satisfied; that is, a flow uniform in velocity and pressure, must remain uniform during its temporal evolution. Fully discrete MF schemes are then designed as follows:

- First, we construct a fully discrete Weakly Implicit MF scheme, denoted as WIMF-AUSM, which employs AUSM type of convective fluxes similar to those used e.g. by Paillére et al [19];
- second, we construct a fully discrete Strongly Implicit MF scheme, denoted as SIMF-AUSM, which also apply convective fluxes of the AUSM type.

In previous works dealing with construction of schemes within the MF framework [12, 11], we have applied AUSMD type of convective schemes similar to those used in [10]. Hence, this work serves to demonstrate some of the flexibility of the MF approach by replacing the AUSMD/V convective fluxes applied in [12, 11] with AUSM type. Roughly speaking, it seems that as long as

we work with convective fluxes which satisfy the requirements of the MF framework, the resulting MF schemes are not very sensitive for the specific choice. The motivation for using AUSM type of fluxes in the present work is that we then naturally can enforce an implicit time discretization which allows us to produce *strongly implicit* schemes as described above.

Many numerical simulations are made to highlight the differences and similarities between WIMF-AUSM and SIMF-AUSM. In particular, we observe the following:

- For timesteps dictated by the sonic CFL condition (2) both schemes give a performance which is similar to an explicit Roe scheme.
- The WIMF-AUSM scheme allows *exact* resolution of a moving contact discontinuity. This property closely hang on the fact that WIMF-type of schemes are stable for timesteps dictated by the weak CFL condition (3). Explicit schemes, like the Roe scheme used in this work for comparison purposes, are excluded from possessing this property since the timestep must obey the strong CFL condition (2).
- The SIMF-AUSM scheme gives numerical mass fluxes similar to the WIMF-AUSM scheme, but does not possess the "exact resolution property" for a linear contact discontinuity due to the implicit discretization of its numerical mass fluxes. On the other hand, this scheme is *unconditionally* stable for a moving linear contact discontinuity, however at a price of introducing a strong smearing of the contact discontinuity.

More generally, the results when WIMF-AUSM and SIMF-AUSM are explored for many different flow cases, indicate that for several cases, the SIMF scheme allows for an increased timestep and improved computational efficiency on a given grid. In particular the SIMF scheme allows for efficient steady state calculations. However, the SIMF is inherently more diffusive than the WIMF on volume fraction waves. This limits the applicability of the SIMF scheme for accurate calculation of slow transients (mass fronts), where a weakly implicit scheme may generally be preferable.

Our paper is organized as follows: In Section 2, the particular two-fluid model we study is presented. In Section 3 we describe the MF approach as developed in [12, 11]. Then, in Section 4 we detail fully discrete numerical schemes by working within the MF frame of Section 3. In particular, we develop a WIMF-AUSM scheme and a SIMF-AUSM scheme. In Section 5 we state some important properties of the SIMF-AUSM and WIMF-AUSM schemes. Finally, in Section 6 we present numerical simulations. Particularly, we demonstrate that the SIMF scheme introduced in this paper is able to violate the CFL criterion for all waves for a wide range of problems, justifying its description as a *strongly implicit* scheme. In Section 6.5 we suggest a slight modification of the SIMF-AUSM scheme consistent with our framework, enabling it to handle the transition to one-phase flow in a stable and accurate manner.

2. The Two-Fluid Model

Throughout this paper we will be concerned with the common two-fluid model formulated by stating separate conservation equations for mass and momentum for the two fluids, which we will denote as a gas (g) and a liquid (l) phase. The model has been studied by several authors [25, 4, 5, 19, 10] and will be briefly stated here. We let $\mathbf{U}$ be the vector of conserved variables

$$\mathbf{U} = \begin{bmatrix} \rho_{\mathrm{g}}\alpha_{\mathrm{g}} \\ \rho_{\mathrm{l}}\alpha_{\mathrm{l}} \\ \rho_{\mathrm{g}}\alpha_{\mathrm{g}}v_{\mathrm{g}} \\ \rho_{\mathrm{l}}\alpha_{\mathrm{l}}v_{\mathrm{l}} \end{bmatrix} = \begin{bmatrix} m_{\mathrm{g}} \\ m_{\mathrm{l}} \\ I_{\mathrm{g}} \\ I_{\mathrm{l}} \end{bmatrix}. \tag{4}$$

By using the notation $\Delta p = p - p^i$, where p^i is the interfacial pressure, and $\tau_k = (p^i - p)\partial_x \alpha_k$, we see that the model (1) can be written on the form

- Conservation of mass

$$\frac{\partial}{\partial t}\left(\rho_{\mathrm{g}}\alpha_{\mathrm{g}}\right) + \frac{\partial}{\partial x}\left(\rho_{\mathrm{g}}\alpha_{\mathrm{g}}v_{\mathrm{g}}\right) = 0, \tag{5}$$

$$\frac{\partial}{\partial t}\left(\rho_{\mathrm{l}}\alpha_{\mathrm{l}}\right) + \frac{\partial}{\partial x}\left(\rho_{\mathrm{l}}\alpha_{\mathrm{l}}v_{\mathrm{l}}\right) = 0, \tag{6}$$

- Conservation of momentum

$$\frac{\partial}{\partial t}\left(\rho_{\mathrm{g}}\alpha_{\mathrm{g}}v_{\mathrm{g}}\right)+\frac{\partial}{\partial x}\left(\rho_{\mathrm{g}}\alpha_{\mathrm{g}}v_{\mathrm{g}}^2\right)+\alpha_{\mathrm{g}}\frac{\partial p}{\partial x}+\Delta p\frac{\partial \alpha_{\mathrm{g}}}{\partial x}=Q_{\mathrm{g}}+M_{\mathrm{g}}^{\mathrm{D}}, \tag{7}$$

$$\frac{\partial}{\partial t}\left(\rho_{\mathrm{l}}\alpha_{\mathrm{l}}v_{\mathrm{l}}\right)+\frac{\partial}{\partial x}\left(\rho_{\mathrm{l}}\alpha_{\mathrm{l}}v_{\mathrm{l}}^2\right)+\alpha_{\mathrm{l}}\frac{\partial p}{\partial x}+\Delta p\frac{\partial \alpha_{\mathrm{l}}}{\partial x}=Q_{\mathrm{l}}+M_{\mathrm{l}}^{\mathrm{D}}. \tag{8}$$

The system is closed by some equation of states (EOS) for the liquid and gas phase. The numerical methods we study in this work allow general expressions for the EOS. However, for the numerical simulations presented in this work we assume the simplified thermodynamic relations

$$\rho_{\mathrm{l}}=\rho_{\mathrm{l},0}+\frac{p-p_0}{a_{\mathrm{l}}^2} \tag{9}$$

and

$$\rho_{\mathrm{g}}=\frac{p}{a_{\mathrm{g}}^2} \tag{10}$$

where

$$p_0=1\text{ bar}=10^5\text{ Pa}$$
$$\rho_{\mathrm{l},0}=1000\text{ kg/m}^3,$$
$$a_{\mathrm{g}}^2=10^5(\mathrm{m/s})^2$$

and

$$a_{\mathrm{l}}=10^3\text{ m/s}.$$

Moreover, we will treat Q_k as a pure source term, assuming that it does not contain any differential operators. We use the interface pressure correction

$$\Delta p=\sigma\frac{\alpha_{\mathrm{g}}\alpha_{\mathrm{l}}\rho_{\mathrm{g}}\rho_{\mathrm{l}}}{\rho_{\mathrm{g}}\alpha_{\mathrm{l}}+\rho_{\mathrm{l}}\alpha_{\mathrm{g}}}(v_{\mathrm{g}}-v_{\mathrm{l}})^2, \tag{11}$$

where unless otherwise stated we set $\sigma=1.2$. This choice ensures that the model is a hyperbolic system of conservation laws, see for instance [25, 5]. Another feature of this model is that it possesses an approximate mixture sound velocity c given by

$$c=\sqrt{\frac{\rho_{\mathrm{l}}\alpha_{\mathrm{g}}+\rho_{\mathrm{g}}\alpha_{\mathrm{l}}}{\frac{\partial\rho_{\mathrm{g}}}{\partial p}\rho_{\mathrm{l}}\alpha_{\mathrm{g}}+\frac{\partial\rho_{\mathrm{l}}}{\partial p}\rho_{\mathrm{g}}\alpha_{\mathrm{l}}}}. \tag{12}$$

We refer to [25, 10] for more details.

Having solved for the conservative variable $\mathbf{U}$, we need to obtain the primitive variables $(\alpha_{\mathrm{g}},p,v_{\mathrm{g}},v_{\mathrm{l}})$. For the pressure variable we see that by writing the volume fraction equation $\alpha_{\mathrm{g}}+\alpha_{\mathrm{l}}=1$ in terms of the conserved variables as

$$\frac{m_{\mathrm{g}}}{\rho_{\mathrm{g}}(p)}+\frac{m_{\mathrm{l}}}{\rho_{\mathrm{l}}(p)}=1, \tag{13}$$

we obtain a relation yielding the pressure $p(m_{\mathrm{g}},m_{\mathrm{l}})$. Using the relatively simple form of EOS given by (9) and (10) the pressure p is found as a positive root of a second order polynomial. For more general EOS we must solve a non-linear system of equations, for instance by using a Newton-Rapson algorithm.

Moreover, the fluid velocities v_{g} and v_{l} are obtained directly from the relations

$$v_{\mathrm{g}}=\frac{U_3}{U_1},\qquad v_{\mathrm{l}}=\frac{U_4}{U_2}.$$

Throughout this work we will study only the isentropic 4-equation model given above, whereas in general energy conservation equations for each phase could also be included. In this respect we are consistent with our previous works [10, 11].

3. A semi-discrete scheme

In this section we construct semi-discrete approximations of the model (5)–(8). In Section 4 we describe fully discrete schemes obtained from the semi-discrete scheme, and in Section 5 we state basic properties possessed by these schemes. Finally, in Section 6 we explore the performance of these fully discrete schemes by studying several well known two-phase flow problems.

3.1. **General form.** It will be convenient to express the model (5)–(8) on the following form:

$$\begin{aligned} \partial_t m_k + \partial_x f_k &= 0, \\ \partial_t I_k + \partial_x g_k + \alpha_k \partial_x p + (\Delta p)\partial_x \alpha_k &= Q_k, \end{aligned} \tag{14}$$

where $k = \mathrm{g}, \mathrm{l}$ and

$$\begin{aligned} f_k &= \rho_k \alpha_k v_k \quad \text{and} \quad m_k = \rho_k \alpha_k \\ g_k &= \rho_k \alpha_k v_k^2 \quad \text{and} \quad I_k = \rho_k \alpha_k v_k. \end{aligned}$$

We assume that we have given approximations $\left(m_{k,j}^n, I_{k,j}^n\right) \approx \left(m_{k,j}(t^n), I_{k,j}(t^n)\right)$. Approximations $m_{k,j}(t)$ and $I_{k,j}(t)$ for $t \in (t^n, t^{n+1}]$ are now constructed by solving the following ODE problem:

$$\begin{aligned} \dot{m}_{k,j} + \delta_x F_{k,j} &= 0, \\ \dot{I}_{k,j} + \delta_x G_{k,j} + \alpha_{k,j}\delta_x P_j + (\Delta p)_j \delta_x \Lambda_{k,j} &= Q_{k,j}, \end{aligned} \tag{15}$$

subject to the initial conditions

$$m_{k,j}(t^n) = m_{k,j}^n, \qquad I_{k,j}(t^n) = I_{k,j}^n.$$

Here δ_x is the operator defined by

$$\delta_x w_j = \frac{w_{j+1/2} - w_{j-1/2}}{\Delta x}, \qquad \delta_x w_{j+1/2} = \frac{w_{j+1} - w_j}{\Delta x},$$

and $(\Delta p)_j(t) = (\Delta p)\left(U_j(t), \delta\right)$ is obtained from (11). Moreover, $F_{k,j+1/2}(t) = F_k(U_j(t), U_{j+1}(t))$, $G_{k,j+1/2}(t) = G_k(U_j(t), U_{j+1}(t))$, $P_{j+1/2}(t) = P(U_j(t), U_{j+1}(t))$, and $\Lambda_{k,j+1/2}(t) = \Lambda_k(U_j(t), U_{j+1}(t))$ are assumed to be numerical fluxes consistent with the corresponding physical fluxes, i.e.

$$\begin{aligned} F_k(U,U) &= f_k = \rho_k \alpha_k v_k \\ G_k(U,U) &= g_k = \rho_k \alpha_k v_k^2 \\ P(U,U) &= p \\ \Lambda_k(U,U) &= \alpha_k. \end{aligned}$$

3.2. **The class of Mixture Flux (MF) methods.** Before we describe the MF approach it will be useful to introduce some basic concepts consistent with those used in [11, 12]. Assume that we consider a contact discontinuity given by

$$\begin{aligned} p_{\mathrm{L}} &= p_{\mathrm{R}} = p \\ \alpha_{\mathrm{L}} &\neq \alpha_{\mathrm{R}} \\ (v_{\mathrm{g}})_{\mathrm{L}} = (v_{\mathrm{l}})_{\mathrm{L}} &= (v_{\mathrm{g}})_{\mathrm{R}} = (v_{\mathrm{l}})_{\mathrm{R}} = v, \end{aligned} \tag{16}$$

for the time period $[t^n, t^{n+1}]$. All pressure terms vanish from the model (5)-(8), and it is seen that the solution to this initial value problem is simply that the discontinuity will propagate with the velocity v. The exact solution of the Riemann problem will then give the numerical mass flux

$$(\rho\alpha v)_{j+1/2} = \frac{1}{2}\rho(\alpha_{\mathrm{L}} + \alpha_{\mathrm{R}})v - \frac{1}{2}\rho(\alpha_{\mathrm{R}} - \alpha_{\mathrm{L}})|v|. \tag{17}$$

Definition 1. *A numerical flux F that satisfy (17) for the contact discontinuity (16) will in the following be termed a "mass coherent" flux.*

Definition 2. *A pair of numerical fluxes $(F_{\mathrm{l}}, F_{\mathrm{g}})$ that satisfy the relation*

$$\rho_{\mathrm{g}} F_{\mathrm{l},j+1/2} + \rho_{\mathrm{l}} F_{\mathrm{g},j+1/2} = \rho_{\mathrm{g}}\rho_{\mathrm{l}} v. \tag{18}$$

for the contact discontinuity (16) will in the following be termed "pressure coherent" fluxes.

Definition 3. *We will use the term* **Mixture Flux** *(MF) methods to denote numerical algorithms which are constructed within the semidiscrete frame of* (15) *where fluxes are given as follows:*

(1) *The numerical flux* $\Lambda_{k,j+1/2}(t)$ *is obtained as*

$$\Lambda_{k,j+1/2}(t) = \frac{\alpha_{k,j}(t) + \alpha_{k,j+1}(t)}{2}. \tag{19}$$

(2) *We determine* $P_{j+1/2}(t)$ *for* $t \in (t^n, t^{n+1}]$ *by solving the ODE*

$$\begin{aligned} &\dot{P}_{j+1/2} + [\kappa_{j+1/2}\rho_{\mathrm{l},j+1/2}]\delta_x I_{\mathrm{g},j+1/2} + [\kappa_{j+1/2}\rho_{\mathrm{g},j+1/2}]\delta_x I_{\mathrm{l},j+1/2} = 0 \\ &P_{j+1/2}(t_+^n) = \frac{p_j^n + p_{j+1}^n}{2}, \end{aligned} \tag{20}$$

where the interface values $\kappa_{j+1/2}$ *and* $\rho_{k,j+1/2}$ *are computed from* $P_{j+1/2}(t)$ *together with the arithmetic average* (19) *which defines* $\alpha_{k,j+1/2}(t)$*. Here* κ *is given by*

$$\kappa = \frac{1}{\frac{\partial \rho_{\mathrm{l}}}{\partial p}\alpha_{\mathrm{l}}\rho_{\mathrm{g}} + \frac{\partial \rho_{\mathrm{g}}}{\partial p}\alpha_{\mathrm{g}}\rho_{\mathrm{l}}}. \tag{21}$$

(3) *We consider hybrid mass fluxes* $F_{k,j+1/2}(t)$ *of the form*

$$F_{\mathrm{l},j+1/2}(t) = \kappa_{j+1/2}(t)\left(\rho_{\mathrm{g}}\alpha_{\mathrm{l}}\frac{\partial \rho_{\mathrm{l}}}{\partial p}F_{\mathrm{l}}^{\mathrm{D}}(t) + \rho_{\mathrm{l}}\alpha_{\mathrm{g}}\frac{\partial \rho_{\mathrm{g}}}{\partial p}F_{\mathrm{l}}^{\mathrm{A}}(t) + \rho_{\mathrm{l}}\alpha_{\mathrm{l}}\frac{\partial \rho_{\mathrm{l}}}{\partial p}(F_{\mathrm{g}}^{\mathrm{D}} - F_{\mathrm{g}}^{\mathrm{A}})(t)\right)_{j+1/2} \tag{22}$$

and

$$F_{\mathrm{g},j+1/2}(t) = \kappa_{j+1/2}(t)\left(\rho_{\mathrm{l}}\alpha_{\mathrm{g}}\frac{\partial \rho_{\mathrm{g}}}{\partial p}F_{\mathrm{g}}^{\mathrm{D}}(t) + \rho_{\mathrm{g}}\alpha_{\mathrm{l}}\frac{\partial \rho_{\mathrm{l}}}{\partial p}F_{\mathrm{g}}^{\mathrm{A}}(t) + \rho_{\mathrm{g}}\alpha_{\mathrm{g}}\frac{\partial \rho_{\mathrm{g}}}{\partial p}(F_{\mathrm{l}}^{\mathrm{D}} - F_{\mathrm{l}}^{\mathrm{A}})(t)\right)_{j+1/2}. \tag{23}$$

The coefficient variables at $j+1/2$ *are determined from the cell interface pressure* $P_{j+1/2}(t)$ *as well as the relation*

$$\alpha_{j+1/2}(t) = \frac{1}{2}(\alpha_j(t) + \alpha_{j+1}(t))$$

which is consistent with the treatment of the coefficients of the pressure evolution equation (20)*.*

(a) *The flux component* $F_k^{\mathrm{A}}(t)$ *is assumed to be consistent with its physical flux* $(\rho\alpha v)_k(t)$ *as well as "mass coherent" in the sense of Definition 1.*
(b) *The flux component* $F_k^{\mathrm{D}}(t)$ *is assumed to be consistent with its physical flux* $(\rho\alpha v)_k(t)$ *as well as "pressure coherent" in the sense of Definition 2.*

(4) *We choose* $G_{k,j+1/2}(t)$ *to be consistent with the flux component* $F_{k,j+1/2}^{\mathrm{A}}(t)$ *in the following sense: For a flow with velocities which are constant in space for the time interval* $[t^n, t^{n+1}]$*, that is,*

$$v_{k,j}(t) = v_{k,j+1}(t) = v_k(t), \qquad t \in [t^n, t^{n+1}], \tag{24}$$

we assume that $G_{k,j+1/2}(t)$ *takes the form*

$$G_{k,j+1/2}(t) = G_{k,j+1/2}^{\mathrm{A}}(t) = v_k(t)F_{k,j+1/2}^{\mathrm{A}}(t), \tag{25}$$

where $F_{k,j+1/2}^{\mathrm{A}}(t)$ *is the numerical flux component introduced above.*

It is easy to check that the above numerical fluxes $\Lambda_{k,j+1/2}$, $P_{j+1/2}$, $F_{k,j+1/2}$, and $G_{k,j+1/2}$ are consistent with the corresponding physical fluxes. We refer to [12] for more details. We now state the following important lemma whose proof can also be found in [12]:

Lemma 1. *Let the mixture fluxes (22) and (23) be constructed from pressure coherent fluxes* F_k^{D} *in the sense of Definition 2, and mass coherent fluxes* F_k^{A} *in the sense of Definition 1. Then the hybrid fluxes (22) and (23) reduce to the upwind fluxes (17) on the contact discontinuity (16), i.e. they are mass coherent.*

It follows directly from Definition 3 and Lemma 1 that

Corollary 1. *The mass fluxes of the MF methods given by Definition 3, are mass coherent in the sense of Definition 1.*

Moreover, by application of Lemma 1 and Definition 3, we can verify that the MF methods satisfy the following principle due to Abgrall [1, 21, 22]:
A flow, uniform in pressure and velocity must remain uniform in the same variables during its time evolution. We refer to [12] for its straightforward proof.

Corollary 2. *The MF methods given by Definition 3, obey Abgrall's principle. More precisely, for the contact discontinuity* (16) *the semidiscrete approximation* (15) *takes the following form*

$$\begin{aligned} \dot{m}_{k,j} + \delta_x(\rho_k \alpha_k v_k)_j &= 0, \\ v\ \dot{m}_{k,j} + v\delta_x(\rho_k \alpha_k v_k)_j &= 0, \end{aligned} \tag{26}$$

where $(\rho_k \alpha_k v_k)_{j+1/2}$ *is on the form* (17). *Consequently, no momentum change is introduced and the contact discontinuity remains unchanged except from experiencing a convective transport.*

In conclusion, Corollary 1 states that the MF mass fluxes recover the numerical fluxes of an exact riemann solver for a moving or stationary contact discontinuity. Corollary 2 ensures that Abgrall's principle [1] is satisfied. The fact that this principle is obeyed, ensures that the use of the pressure evolution equation (20) in the discretization of the non-conservative pressure term is consistent with basic physical understanding of two-phase flow phenomena.

Remark 1. *The following differential relations are obtained from the basic relation* (13) *(see* [12, 11] *for more details):*

$$\begin{aligned} dp &= \kappa(\rho_{\mathrm{l}} dm_{\mathrm{g}} + \rho_{\mathrm{g}} dm_{\mathrm{l}}) \\ d\alpha_{\mathrm{l}} &= \kappa(-\frac{\partial \rho_{\mathrm{l}}}{\partial p}\alpha_{\mathrm{l}} dm_{\mathrm{g}} + \frac{\partial \rho_{\mathrm{g}}}{\partial p}\alpha_{\mathrm{g}} dm_{\mathrm{l}}), \end{aligned} \tag{27}$$

where κ *is given by* (21) *and*

$$\begin{aligned} dm_{\mathrm{g}} &= \alpha_{\mathrm{g}} \frac{\partial \rho_{\mathrm{g}}}{\partial p} dp - \rho_{\mathrm{g}} d\alpha_{\mathrm{l}} \\ dm_{\mathrm{l}} &= \alpha_{\mathrm{l}} \frac{\partial \rho_{\mathrm{l}}}{\partial p} dp + \rho_{\mathrm{l}} d\alpha_{\mathrm{l}}. \end{aligned} \tag{28}$$

Multiplying the gas mass conservation equation by $\kappa\rho_{\mathrm{l}}$ *and the liquid mass conservation equation by* $\kappa\rho_{\mathrm{g}}$ *and then adding the two resulting equations, yields the equation*

$$\kappa\rho_{\mathrm{l}} \frac{\partial}{\partial t} m_{\mathrm{g}} + \kappa\rho_{\mathrm{g}} \frac{\partial}{\partial t} m_{\mathrm{l}} + \kappa\rho_{\mathrm{l}} \frac{\partial}{\partial x}(\rho_{\mathrm{g}} \alpha_{\mathrm{g}} v_{\mathrm{g}}) + \kappa\rho_{\mathrm{g}} \frac{\partial}{\partial x}(\rho_{\mathrm{l}} \alpha_{\mathrm{l}} v_{\mathrm{l}}) = 0.$$

In view of the first equation of (27), *the pressure evolution equation* (20) *follows.*

The mixture mass fluxes (22) *and* (23) *are obtained by first introducing a flux component* F_p *(associated with the pressure) and* F_α *(associated with the volume fraction) such that the mass fluxes* F_{l} *and* F_{g}, *inspired by* (28), *are given by*

$$\begin{aligned} F_{\mathrm{l}} &= \alpha_{\mathrm{l}} \frac{\partial \rho_{\mathrm{l}}}{\partial p} F_p + \rho_{\mathrm{l}} F_\alpha \\ F_{\mathrm{g}} &= \alpha_{\mathrm{g}} \frac{\partial \rho_{\mathrm{g}}}{\partial p} F_p - \rho_{\mathrm{g}} F_\alpha. \end{aligned} \tag{29}$$

Inspired by the differential relations (27) *we propose to give* F_p *and* F_α *the following form*

$$\begin{aligned} F_p &= \kappa\rho_{\mathrm{g}} F_{\mathrm{l}}^{\mathrm{D}} + \kappa\rho_{\mathrm{l}} F_{\mathrm{g}}^{\mathrm{D}} \\ F_\alpha &= \kappa \frac{\partial \rho_{\mathrm{g}}}{\partial p} \alpha_{\mathrm{g}} F_{\mathrm{l}}^{\mathrm{A}} - \kappa \frac{\partial \rho_{\mathrm{l}}}{\partial p} \alpha_{\mathrm{l}} F_{\mathrm{g}}^{\mathrm{A}}, \end{aligned} \tag{30}$$

where $F_{\mathrm{k}}^{\mathrm{D}}$ *should possess the "pressure coherent" property whereas* $F_{\mathrm{k}}^{\mathrm{A}}$ *should possess the "mass coherent" property. Combining* (29) *and* (30) *yields the mixture mass fluxes* (22) *and* (23).

It will be useful to introduce the following two definitions of the terms *weakly implicit* and *strongly implicit*:

Definition 4. *Assume that we initially are given a contact discontinuity* (16). *A numerical scheme is said to be* **weakly implicit** *if it allows stable calculation of solutions under the CFL condition*

$$\frac{\Delta x}{\Delta t} \geq |v|. \tag{31}$$

Definition 5. *Assume that we initially are given a contact discontinuity* (16). *A numerical scheme is said to be* **strongly implicit** *if it allows stable calculation of solutions under no restriction on the time step.*

Remark 2. *Note that the time step restriction* (31) *is consistent with the CFL condition* (3). *This follows from the fact that for the contact discontinuity* (16) *the two eigenvalues corresponding to volume fraction waves degenerate and coincide with fluid velocity* v. *We refer to* [10] *for more details concerning the eigenvalue structure of the two-fluid model under considerations.*

4. Fully Discrete Numerical Schemes

The purpose of this section is to construct fully discrete schemes based on the general class of MF schemes given by Definition 3. We first describe how to construct appropriate candidates for the mass flux components F_k^{A} and F_k^{D} which were introduced in Definition 3. Then we apply these components to propose fully discrete schemes, one type which is denoted as *Weakly Implicit Mixture Flux* (WIMF) and another denoted as *Strongly Implicit Mixture Flux* (SIMF). Both schemes contain the mechanism which allows us to obtain stable pressure calculation for large time steps. The difference between them lies in the temporal discretization of the mass fluxes, more precisely, the F_k^{A} mass flux component.

4.1. A pressure coherent convective mass flux F_k^{D}.

Due to the fact that the mass flux component F_k^{D} is associated with the pressure calculation as described in Remark 1, it is natural to choose a discretization of this flux which is consistent with the discretization of the pressure evolution equation. On the semi-discrete level, in view of (20), we therefore propose to consider the following discretization of the mass conservation equations

$$\begin{aligned} \dot{m}_{k,j+1/2} + \delta_x I_{k,j+1/2} &= 0, \qquad t \in (t^n, t^{n+1}] \\ m_{k,j+1/2}(t_+^n) &= \frac{m_{k,j}^n + m_{k,j+1}^n}{2}. \end{aligned} \tag{32}$$

We now suggest to average as follows:

$$m_{k,j}(t) = \frac{1}{2}\left(m_{k,j-1/2}(t) + m_{k,j+1/2}(t)\right),$$

which implies that

$$\dot{m}_{k,j}\,(t) = \frac{1}{2}\left(\dot{m}_{k,j-1/2}\,(t) + \dot{m}_{k,j+1/2}\,(t)\right). \tag{33}$$

By substituting (32) into (33) we obtain the following ODE equation for $m_{k,j}(t)$:

$$\begin{aligned} \dot{m}_{k,j} + \frac{1}{2\Delta x}(I_{k,j+1} - I_{k,j-1}) &= 0, \qquad t \in (t^n, t^{n+1}] \\ m_{k,j}(t_+^n) &= \frac{1}{4}\Big(m_{k,j-1}^n + 2m_{k,j}^n + m_{k,j+1}^n\Big). \end{aligned} \tag{34}$$

This equation is the basis for designing the flux component $F_{k,j+1/2}^{\mathrm{D}}$. A fully discrete version of (34) which employs updated mass fluxes $I_{k,j}^{n+1}$ is given by

$$\frac{m_{k,j}^{n+1} - \frac{1}{4}\left(2m_{k,j}^n + m_{k,j-1}^n + m_{k,j+1}^n\right)}{\Delta t} + \frac{1}{2\Delta x}\left(I_{k,j+1}^{n+1} - I_{k,j-1}^{n+1}\right) = 0. \tag{35}$$

This equation can be written on the flux-conservative form

$$m_{k,j}^{n+1} = m_{k,j}^n - \frac{\Delta t}{\Delta x}\delta_x (F_k^{\mathrm{D}})_j^{n+1/2},$$

where

$$(F_k^{\mathrm{D}})_{j+1/2}^{n+1/2} = \frac{1}{2}(I_{k,j}^{n+1} + I_{k,j+1}^{n+1}) + \frac{1}{4}\frac{\Delta x}{\Delta t}(m_{k,j}^n - m_{k,j+1}^n). \tag{36}$$

We can easily check that the proposed flux F_k^{D} possesses the "pressure coherent" property of Definition 2, see [12, 11].

Proposition 1. *The flux component F_k^{D} given by* (36) *is pressure coherent in the sense of Definition 2.*

Remark 3. *The motivation for enforcing an implicit treatment of the terms I_k in the mass fluxes* (36) *is to free the resulting schemes from the strong CFL condition* (2)*. In* [12] *we studied explicit MF schemes where the mass flux F_k^{D} was given the pure explicit form*

$$(F_k^{\mathrm{D}})_{j+1/2}^{n} = \frac{1}{2}(I_{k,j}^{n} + I_{k,j+1}^{n}) + \frac{1}{4}\frac{\Delta x}{\Delta t}(m_{k,j}^n - m_{k,j+1}^n). \tag{37}$$

The main difference between using (36) *and* (37) *is that that* (36) *introduces a stronger smearing of the sonic waves, see* [11]*. On the other hand,* (37) *does not allow the resulting MF schemes to break the strong CFL condition* (2)*.*

4.2. Convective fluxes $F_k^{\mathbf{A}}$ and $G_k^{\mathbf{A}}$.

4.2.1. *FVS.* For an FVS type of scheme, the convective flux terms are split into upstream and downstream travelling components as

$$\mathbf{F}(\mathbf{U}) = \mathbf{F}^+(\mathbf{U}) + \mathbf{F}^-(\mathbf{U}), \tag{38}$$

where $\mathbf{F} = (\rho\alpha v, \rho\alpha v^2)^T$ so that the numerical flux at the interface $j+1/2$ is given as

$$\mathbf{F}_{j+1/2} = \mathbf{F}(\mathbf{U}_{\mathrm{L}}, \mathbf{U}_{\mathrm{R}}) = \mathbf{F}^+(\mathbf{U}_{\mathrm{L}}) + \mathbf{F}^-(\mathbf{U}_{\mathrm{R}}). \tag{39}$$

We consider the velocity splitting formulas used in previous works [15, 27, 8, 9, 10]

$$V^{\pm}(v,c) = \begin{cases} \pm\frac{1}{4c}(v \pm c)^2 & \text{if } |v| \le c \\ \frac{1}{2}(v \pm |v|) & \text{otherwise} \end{cases}, \tag{40}$$

where the parameter c represents the physical sound velocity for the system. For the two-fluid model, we assume that it is given by the approximate expression (12). We define a cell interface sound velocity $c_{j+1/2}$ as follows

$$c_{j+1/2} = \max(c_j, c_{j+1}). \tag{41}$$

We now let the numerical fluxes be given as follows

(1) *Mass Flux.* We let the numerical mass flux $(\rho\alpha v)_{j+1/2}$ be given as

$$(\rho\alpha v)_{j+1/2} = (\rho\alpha)_j V^+(v_j, c_{j+1/2}) + (\rho\alpha)_{j+1} V^-(v_{j+1}, c_{j+1/2}) \tag{42}$$

for each phase.

(2) *Momentum Flux.* We let the numerical convective momentum flux $(\rho\alpha v^2)_{j+1/2}$ be given as

$$(\rho\alpha v^2)_{j+1/2} = (\rho\alpha v)_j V^+(v_j, c_{j+1/2}) + (\rho\alpha v)_{j+1} V^-(v_{j+1}, c_{j+1/2}). \tag{43}$$

4.2.2. *AUSM.* We define a cell interface velocity $v_{j+1/2}$ as

$$v_{j+1/2} = V^+(v_j, c_{j+1/2}) + V^-(v_{j+1}, c_{j+1/2}), \tag{44}$$

and obtain the convective fluxes as

$$(\rho\alpha v)_{j+1/2} = \begin{cases} (\rho\alpha)_j v_{j+1/2} & \text{if } v_{j+1/2} \ge 0 \\ (\rho\alpha)_{j+1} v_{j+1/2} & \text{otherwise} \end{cases} \tag{45}$$

and

$$(\rho\alpha v^2)_{j+1/2} = \begin{cases} (\rho\alpha v)_j v_{j+1/2} & \text{if } v_{j+1/2} \ge 0 \\ (\rho\alpha v)_{j+1} v_{j+1/2} & \text{otherwise.} \end{cases} \tag{46}$$

In the following we use AUSM convective fluxes as bases to define MF type of schemes. It is straightforward to check that AUSM possesses the "mass coherent" property.

Proposition 2. *The convective flux $(\rho\alpha v)_{j+1/2}^{\mathrm{AUSM}}$ is mass coherent in the sense of Definition 1.*

The FVS convective mass fluxes are pressure coherent but not mass coherent. Consequently, they are not accurate for a moving or steady contact discontinuity [10]. However, the FVS convective fluxes are very stable and will be introduced in an appropriate manner when we study flows which involve transition to single-phase flow. We refer to Section 6.5 for details.

4.3. **A Weakly Implicit Mixture Flux (WIMF) Scheme.**

4.3.1. *General form.* We use the shorthands $m_k = \rho_k \alpha_k$ and $I_k = m_k v_k$ and consider a fully discrete scheme based on (15) given as follows.

- Gas Mass
$$\frac{m_{\mathrm{g},j}^{n+1} - m_{\mathrm{g},j}^{n}}{\Delta t} = -\delta_x F_{\mathrm{g},j}^{n+1/2} \tag{47}$$
- Liquid Mass
$$\frac{m_{\mathrm{l},j}^{n+1} - m_{\mathrm{l},j}^{n}}{\Delta t} = -\delta_x F_{\mathrm{l},j}^{n+1/2} \tag{48}$$
- Gas Momentum
$$\begin{aligned} &\frac{I_{\mathrm{g},j}^{n+1} - I_{\mathrm{g},j}^{n}}{\Delta t} \\ &= -\delta_x (G^{\mathrm{A}})_{\mathrm{g},j}^{n} - \alpha_{\mathrm{g},j}^{n} \frac{P_{j+1/2}^{n+1} - P_{j-1/2}^{n+1}}{\Delta x} - (\Delta p)_j^n \delta_x \Lambda_{\mathrm{g},j}^{n} + (Q_{\mathrm{g}})_j^n. \end{aligned} \tag{49}$$
- Liquid Momentum
$$\begin{aligned} &\frac{I_{\mathrm{l},j}^{n+1} - I_{\mathrm{l},j}^{n}}{\Delta t} \\ &= -\delta_x (G^{\mathrm{A}})_{\mathrm{l},j}^{n} - \alpha_{\mathrm{l},j}^{n} \frac{P_{j+1/2}^{n+1} - P_{j-1/2}^{n+1}}{\Delta x} - (\Delta p)_j^n \delta_x \Lambda_{\mathrm{l},j}^{n} + (Q_{\mathrm{l}})_j^n. \end{aligned} \tag{50}$$

4.3.2. *WIMF-AUSM.*

Definition 6. *We will use the term* **WIMF-AUSM** *to denote the numerical algorithm which is constructed within the discrete frame of* (47)–(50) *where fluxes are given as follows:*

(1) *The numerical flux* $\Lambda_{k,j+1/2}^{n}$ *is obtained as*
$$\Lambda_{k,j+1/2}^{n} = \frac{\alpha_{k,j}^{n} + \alpha_{k,j+1}^{n}}{2}. \tag{51}$$

(2) *We determine* $P_{j+1/2}^{n+1}$ *by considering the following discretization of the pressure evolution equation* (20)
$$\begin{aligned} &\frac{P_{j+1/2}^{n+1} - \frac{1}{2}(p_j^n + p_{j+1}^n)}{\Delta t} \\ &= -(\kappa\rho_{\mathrm{l}})_{j+1/2}^{n} \frac{I_{\mathrm{g},j+1}^{n+1} - I_{\mathrm{g},j}^{n+1}}{\Delta x} - (\kappa\rho_{\mathrm{g}})_{j+1/2}^{n} \frac{I_{\mathrm{l},j+1}^{n+1} - I_{\mathrm{l},j}^{n+1}}{\Delta x}, \end{aligned} \tag{52}$$
where the interface values $\kappa_{j+1/2}^{n}$ *and* $\rho_{k,j+1/2}^{n}$ *are computed from* $P_{j+1/2}^{n}$ *together with the arithmetic average* (51) *which defines* $\alpha_{k,j+1/2}^{n}$.

(3) *We consider hybrid mass fluxes* $F_{k,j+1/2}^{n+1/2}$ *of the form*
$$F_{\mathrm{l},j+1/2}^{n+1/2} = \Big([\kappa\rho_{\mathrm{g}}\alpha_{\mathrm{l}}\partial_p\rho_{\mathrm{l}}]^n F_{\mathrm{l}}^{\mathrm{D},n+1/2} + [\kappa\rho_{\mathrm{l}}\alpha_{\mathrm{g}}\partial_p\rho_{\mathrm{g}}]^n F_{\mathrm{l}}^{\mathrm{A},n} + [\kappa\rho_{\mathrm{l}}\alpha_{\mathrm{l}}\partial_p\rho_{\mathrm{l}}]^n (F_{\mathrm{g}}^{\mathrm{D},n+1/2} - F_{\mathrm{g}}^{\mathrm{A},n}) \Big)_{j+1/2} \tag{53}$$
and
$$F_{\mathrm{g},j+1/2}^{n+1/2} = \Big([\kappa\rho_{\mathrm{l}}\alpha_{\mathrm{g}}\partial_p\rho_{\mathrm{g}}]^n F_{\mathrm{g}}^{\mathrm{D},n+1/2} + [\kappa\rho_{\mathrm{g}}\alpha_{\mathrm{l}}\partial_p\rho_{\mathrm{l}}]^n F_{\mathrm{g}}^{\mathrm{A},n} + [\kappa\rho_{\mathrm{g}}\alpha_{\mathrm{g}}\partial_p\rho_{\mathrm{g}}]^n (F_{\mathrm{l}}^{\mathrm{D},n+1/2} - F_{\mathrm{l}}^{\mathrm{A},n}) \Big)_{j+1/2}. \tag{54}$$

The coefficient variables at $j+1/2$ are determined from the cell interface pressure $P^n_{j+1/2}$ as well as the relation

$$\alpha^n_{j+1/2} = \frac{1}{2}(\alpha^n_j + \alpha^n_{j+1})$$

which is consistent with the treatment of the coefficients of the pressure evolution equation (52).

(a) *For the flux component $F^{\mathrm{A},n}_{k,j+1/2}$ we refer to Section 4.2 and use*

$$F^{\mathrm{A},n}_{k,j+1/2} = (\rho\alpha v)^{\mathrm{AUSM},n}_{k,j+1/2} = \begin{cases} (\rho\alpha)^n_{k,j} v^n_{k,j+1/2} & \text{if } v^n_{k,j+1/2} \geq 0 \\ (\rho\alpha)^n_{k,j+1} v^n_{k,j+1/2} & \text{otherwise.} \end{cases} \tag{55}$$

(b) *For the flux component $F^{\mathrm{D},n+1/2}_{k,j+1/2}$ we refer to Section 4.1 and use*

$$F^{\mathrm{D},n+1/2}_{k,j+1/2} = \frac{1}{2}(I^{n+1}_{k,j} + I^{n+1}_{k,j+1}) + \frac{1}{4}\frac{\Delta x}{\Delta t}(m^n_{k,j} - m^n_{k,j+1}). \tag{56}$$

(4) *The flux component $G^n_{k,j+1/2}$ is chosen to be consistent with the flux component $F^{\mathrm{A},n}_{k,j+1/2}$ by using*

$$G^n_{k,j+1/2} = G^{\mathrm{A},n}_{k,j+1/2} = (\rho\alpha v^2)^{\mathrm{AUSM},n}_{k,j+1/2} = \begin{cases} (\rho\alpha v)^n_{k,j} v^n_{k,j+1/2} & \text{if } v^n_{k,j+1/2} \geq 0 \\ (\rho\alpha v)^n_{k,j+1} v^n_{k,j+1/2} & \text{otherwise.} \end{cases} \tag{57}$$

4.4. **Two Strongly Implicit Mixture Flux (SIMF) Schemes.**

4.4.1. *General form.* We use the shorthands $m_k = \rho_k\alpha_k$ and $I_k = m_k v_k$ and consider a fully discrete scheme based on (15) given as follows.

- Gas Mass

$$\frac{m^{n+1}_{\mathrm{g},j} - m^n_{\mathrm{g},j}}{\Delta t} = -\delta_x F^{n+1}_{\mathrm{g},j} \tag{58}$$

- Liquid Mass

$$\frac{m^{n+1}_{\mathrm{l},j} - m^n_{\mathrm{l},j}}{\Delta t} = -\delta_x F^{n+1}_{\mathrm{l},j} \tag{59}$$

- Gas Momentum

$$\begin{aligned} &\frac{I^{n+1}_{\mathrm{g},j} - I^n_{\mathrm{g},j}}{\Delta t} \\ &= -\delta_x (G^{\mathrm{A}})^{n+1}_{\mathrm{g},j} - \alpha^n_{\mathrm{g},j}\frac{P^{n+1}_{j+1/2} - P^{n+1}_{j-1/2}}{\Delta x} - (\Delta p)^n_j \delta_x \Lambda^n_{\mathrm{g},j} + (Q_{\mathrm{g}})^n_j. \end{aligned} \tag{60}$$

- Liquid Momentum

$$\begin{aligned} &\frac{I^{n+1}_{\mathrm{l},j} - I^n_{\mathrm{l},j}}{\Delta t} \\ &= -\delta_x (G^{\mathrm{A}})^{n+1}_{\mathrm{l},j} - \alpha^n_{\mathrm{l},j}\frac{P^{n+1}_{j+1/2} - P^{n+1}_{j-1/2}}{\Delta x} - (\Delta p)^n_j \delta_x \Lambda^n_{\mathrm{l},j} + (Q_{\mathrm{l}})^n_j. \end{aligned} \tag{61}$$

4.4.2. *SIMF-AUSM.*

Definition 7. *We will use the term* **SIMF-AUSM** *to denote the numerical algorithm which is constructed within the discrete frame of* (58)–(61) *where fluxes are given as follows:*

(1) *The numerical flux $\Lambda^n_{k,j+1/2}$ is defined as in* (51).
(2) *We determine $P^{n+1}_{j+1/2}$ by considering the discretization* (52) *of the pressure evolution equation* (20)
(3) *We consider hybrid mass fluxes $F^{n+1}_{k,j+1/2}$ of the form*

$$F^{n+1}_{\mathrm{l},j+1/2} = \Big([\kappa\rho_{\mathrm{g}}\alpha_{\mathrm{l}}\partial_p\rho_{\mathrm{l}}]^n F^{\mathrm{D},n+1/2}_{\mathrm{l}} + [\kappa\rho_{\mathrm{l}}\alpha_{\mathrm{g}}\partial_p\rho_{\mathrm{g}}]^n F^{\mathrm{A},n+1}_{\mathrm{l}} + [\kappa\rho_{\mathrm{l}}\alpha_{\mathrm{l}}\partial_p\rho_{\mathrm{l}}]^n (F^{\mathrm{D},n+1/2}_{\mathrm{g}} - F^{\mathrm{A},n+1}_{\mathrm{g}})\Big)_{j+1/2} \tag{62}$$

and

$$F^{n+1/2}_{\mathrm{g},j+1/2} = \Big([\kappa\rho_{\mathrm{l}}\alpha_{\mathrm{g}}\partial_p\rho_{\mathrm{g}}]^n F^{\mathrm{D},n+1/2}_{\mathrm{g}} + [\kappa\rho_{\mathrm{g}}\alpha_{\mathrm{l}}\partial_p\rho_{\mathrm{l}}]^n F^{\mathrm{A},n+1}_{\mathrm{g}} + [\kappa\rho_{\mathrm{g}}\alpha_{\mathrm{g}}\partial_p\rho_{\mathrm{g}}]^n (F^{\mathrm{D},n+1/2}_{\mathrm{l}} - F^{\mathrm{A},n+1}_{\mathrm{l}}) \Big)_{j+1/2}. \tag{63}$$

The coefficient variables at $j+1/2$ are determined from the cell interface pressure $P^n_{j+1/2}$ as well as the relation

$$\alpha^n_{j+1/2} = \frac{1}{2}(\alpha^n_j + \alpha^n_{j+1})$$

which is consistent with the treatment of the coefficients of the pressure evolution equation (52).

(a) *For the flux component $F^{\mathrm{A},n+1}_{k,j+1/2}$ we use*

$$F^{\mathrm{A},n+1}_{k,j+1/2} = (\rho\alpha v)^{\mathrm{AUSM},n+1}_{k,j+1/2} = \begin{cases} (\rho\alpha)^{n+1}_{k,j} v^n_{k,j+1/2} & \text{if } v^n_{k,j+1/2} \geq 0 \\ (\rho\alpha)^{n+1}_{k,j+1} v^n_{k,j+1/2} & \text{otherwise.} \end{cases} \tag{64}$$

(b) *For the flux component $F^{\mathrm{D},n+1/2}_{k,j+1/2}$ we use*

$$F^{\mathrm{D},n+1/2}_{k,j+1/2} = \frac{1}{2}(I^{n+1}_{k,j} + I^{n+1}_{k,j+1}) + \frac{1}{4}\frac{\Delta x}{\Delta t}(m^n_{k,j} - m^n_{k,j+1}). \tag{65}$$

(4) *The flux component $G^{n+1}_{k,j+1/2}$ is chosen to be consistent with the flux component $F^{\mathrm{A},n+1}_{k,j+1/2}$ by using*

$$G^{n+1}_{k,j+1/2} = G^{\mathrm{A},n+1}_{k,j+1/2} = (\rho\alpha v^2)^{\mathrm{AUSM},n+1}_{k,j+1/2} = \begin{cases} (\rho\alpha v)^{n+1}_{k,j} v^n_{k,j+1/2} & \text{if } v^n_{k,j+1/2} \geq 0 \\ (\rho\alpha v)^{n+1}_{k,j+1} v^n_{k,j+1/2} & \text{otherwise.} \end{cases} \tag{66}$$

4.4.3. *SIMF-FVS.*

Definition 8. *We will use the term* **SIMF-FVS** *to denote the numerical algorithm which is identical to* **SIMF-AUSM** *except from the convective flux terms $F^{\mathrm{A},n+1}_{k,j+1/2}$ and $G^{\mathrm{A},n+1}_{k,j+1/2}$ which are defined as follows:*

(a) *For the flux component $F^{\mathrm{A},n+1}_{k,j+1/2}$ we use*

$$F^{\mathrm{A},n+1}_{k,j+1/2} = (\rho\alpha v)^{\mathrm{FVS},n+1}_{k,j+1/2} = (\rho\alpha)^{n+1}_{k,j} V^+(v^n_{k,j}, c^n_{j+1/2}) + (\rho\alpha)^{n+1}_{k,j+1} V^-(v^n_{k,j+1}, c^n_{j+1/2}). \tag{67}$$

(b) *For the flux component $G^{\mathrm{A},n+1}_{k,j+1/2}$ we use*

$$G^{\mathrm{A},n+1}_{k,j+1/2} = (\rho\alpha v^2)^{\mathrm{FVS},n+1}_{k,j+1/2} = (\rho\alpha v)^{n+1}_{k,j} V^+(v^n_{k,j}, c^n_{j+1/2}) + (\rho\alpha v)^{n+1}_{k,j+1} V^-(v^n_{k,j+1}, c^n_{j+1/2}). \tag{68}$$

Some comments are in order.

Remark 4. *The MF approach, as reflected by the above* **WIMF** *and* **SIMF** *schemes, allows for sequential updating of the conservative variables in the following manner:*

(1) *For both schemes the momentum equations (49) and (50) are solved coupled with the pressure equation* (52) *to yield $p^{n+1}_{j+1/2}$ and $I^{n+1}_{k,j}$.*

(2) *For* **WIMF** *the mass equations (47) and (48) with the mixture fluxes* (53) *and* (54) *are solved separately and in an explicit manner whereas for* **SIMF** *the mass equations (58) and (59) with the mixture fluxes* (62) *and* (63) *are solved coupled with each other to yield $m^{n+1}_{k,j}$.*

In this respect our strongly implicit schemes **(SIMF)** *resemble the schemes used in common industrial codes* [3, 13]. *Advantages of the current schemes include:*

- *The use of the hybrid FVS/FDS convective fluxes allows for solving the conservative variables on a nonstaggered grid.*
- *The central pressure flux F^D_k and the stronger coupling between the mass equations allow for nonoscillatory resolution of the pressure for large timesteps.*

- *The conservative momentum variables I_k are solved for directly, and there is automatic consistency between the pressure and mass variables.*

An advantage of using the AUSM and FVS fluxes described above is that they are linear with respect to their arguments $(\rho\alpha)_{k,j}^{n+1}$ and $(\rho\alpha v)_{k,j}^{n+1}$. Hence only one matrix inversion (per set of equations) is required to solve the resulting system exactly.

5. Properties of the fully discrete MF schemes

In view of Definitions 6 and 7 and Proposition 1 and Proposition 2 it follows that both the WIMF-AUSM and SIMF-AUSM scheme are MF schemes in the sense of Definition 3. Consequently, Corollary 1 and 2 are applicable, and we immediately conclude that

Proposition 3. *WIMF-AUSM and SIMF-AUSM satisfy the following properties:*
(i) The mass fluxes of WIMF-AUSM and SIMF-AUSM are mass coherent in the sense of Definition 1. (ii) Both schemes obey Abgrall's principle.

More precisely, for the contact discontinuity (16) the mass fluxes of WIMF-AUSM take the form

$$(\rho\alpha v)_{k,j+1/2}^{\mathrm{WIMF-AUSM},n+1/2} = \rho_k \alpha_{k,j}^n v, \tag{69}$$

whereas SIMF-AUSM gives mass fluxes on the form

$$(\rho\alpha v)_{k,j+1/2}^{\mathrm{SIMF-AUSM},n+1} = \rho_k \alpha_{k,j}^{n+1} v, \tag{70}$$

where we have assumed (without loss of generality) that $v > 0$. The term *mass coherent* of Definition 1 does not take into account the temporal aspect of the discretization and both schemes are classified as "mass coherent" since they produce the correct upwind form.

The purpose of the next paragraph is to focus on this temporal aspect and provide some insight into a special feature possessed by WIMF type of schemes concerning the ability to resolve a linear contact discontinuity (16) accurately.

5.1. Resolution of moving or stationary contact discontinuity.

We now take a closer look at the contact discontinuity given by (16). We consider a WIMF scheme where the flux component F_k^{A} is mass coherent in the sense of Definition 1. Then, as noted above, we obtain the mass fluxes

$$(\rho_k \alpha_k v_k)_{j+1/2}^{n+1/2} = \rho_k \alpha_{k,j}^n v, \tag{71}$$

where we have assumed that $v \geq 0$.

The discrete evolution equation for the mass at cell j is given by

$$\frac{(\rho_k\alpha_k)_j^{n+1} - (\rho_k\alpha_k)_j^n}{\Delta t} = v\frac{(\rho_k\alpha_k)_{j-1}^n - (\rho_k\alpha_k)_j^n}{\Delta x}. \tag{72}$$

Using that ρ_k is constant, this may be simplified to yield the discrete evolution equation for the volume fractions. For simplicity in notation we drop the phase index k and obtain

$$\frac{\alpha_j^{n+1} - \alpha_j^n}{\Delta t} = v\frac{\alpha_{j-1}^n - \alpha_j^n}{\Delta x}. \tag{73}$$

If the contact discontinuity is exactly reproduced within the grid at time $t^n = n\Delta t$, the discrete representation may be expressed as

$$\begin{aligned} \alpha_j^n &= \alpha_{\mathrm{L}} \qquad \text{for} \qquad j < i, \\ \alpha_j^n &= \alpha_{\mathrm{R}} \qquad \text{for} \qquad j \geq i \end{aligned} \tag{74}$$

for some i. We remember that here $v_{k,j} \equiv v$ and $p_j \equiv p$. From (73) we see that for such an exactly reproduced discontinuity, only the value α_i will change by stepping forward in time from n to $n+1$. We then obtain

$$\frac{\alpha_i^{n+1} - \alpha_{\mathrm{R}}}{\Delta t} = v\frac{\alpha_{\mathrm{L}} - \alpha_{\mathrm{R}}}{\Delta x}. \tag{75}$$

In particular, if $\Delta x/\Delta t = v$ we obtain an interesting result. Then

$$\alpha_i^{n+1} - \alpha_{\mathrm{R}} = \alpha_{\mathrm{L}} - \alpha_{\mathrm{R}} \tag{76}$$

or simply

$$\alpha_i^{n+1} = \alpha_{\mathrm{L}}, \tag{77}$$

whereas

$$\alpha_i^{n} = \alpha_{\mathrm{R}}. \tag{78}$$

So we conclude that integrating the contact discontinuity (74) using the timestep $\Delta x/\Delta t = v$ will simply shift the location of the discontinuity exactly one grid cell to the right. This is exactly the distance the contact discontinuity will move in one timestep, $\Delta x = v\Delta t$. The discrete volume fraction distribution is now given as

$$\begin{aligned} \alpha_j^{n+1} &= \alpha_{\mathrm{L}} \qquad \text{for} \qquad j < i+1, \\ \alpha_j^{n+1} &= \alpha_{\mathrm{R}} \qquad \text{for} \qquad j \geq i+1, \end{aligned} \tag{79}$$

and by induction

$$\begin{aligned} \alpha_j^{n+m} &= \alpha_{\mathrm{L}} \qquad \text{for} \qquad j < i+m, \\ \alpha_j^{n+m} &= \alpha_{\mathrm{R}} \qquad \text{for} \qquad j \geq i+m \end{aligned} \tag{80}$$

for all m (within the boundaries of the grid). We may now state the following lemma

Lemma 2. *Consider a WIMF type of scheme as described in Section 4.3 which is mass coherent in the sense of Definition 1. Apply the WIMF scheme to a contact discontinuity moving with the velocity v, as described by* (16)*. If the optimal timestep $\Delta x/\Delta t = |v|$ is used, the WIMF scheme will exactly capture the contact discontinuity for all $t^n > t^0$.*

Proof. The above discussion proves the Lemma for $v \geq 0$. Repeating the steps for $v < 0$ completes the proof. □

Some remarks are now in order.

Remark 5. *Notably the proof of Lemma 2 does not rely directly upon the scheme being of the WIMF class. An explicit scheme (like the basic AUSMD scheme studied in* [10]*, or the MF-AUSMD scheme considered in* [12]*) which correctly reduces to the upwind scheme for the contact discontinuity* (16) *will also formally satisfy Lemma 2. However, in practice such schemes will not work as they are unstable under the violation of the sonic CFL criterion implied by the timestep $\Delta x/\Delta t = v$. This means that slight numerical oscillations will grow exponentially into instabilities. Even for the above case with a linear contact discontinuity, such numerical errors are expected due to the limited floating point precision of computers.*

For the WIMF class of schemes however, the presence of the implicit flux component F_k^{D} as given by (56) *will prevent the development of such instabilities.*

The ability to exactly capture a contact discontinuity in a stable manner is a very desirable feature unique to the class of WIMF schemes. Numerical evidence of this fact will also be provided in the next section.

Remark 6. *Lemma 2 does not apply to the SIMF class of mass coherent schemes as described in Section 4.4. In this case, the numerical mass flux becomes*

$$(\rho_k \alpha_k v)_{j+1/2}^{n+1} = \rho_k \alpha_{k,j}^{n+1} v \tag{81}$$

for a contact discontinuity of the form (16)*, and* (73) *must be replaced by*

$$\frac{\alpha_j^{n+1} - \alpha_j^n}{\Delta t} = v \frac{\alpha_{j-1}^{n+1} - \alpha_j^{n+1}}{\Delta x}. \tag{82}$$

Hence SIMF operates on a contact discontinuity much the same way as an implicit upwind scheme operates on a scalar advection equation. That is, we expect the SIMF class of schemes to be stable, yet diffusive. This issue is explored in the numerical section.

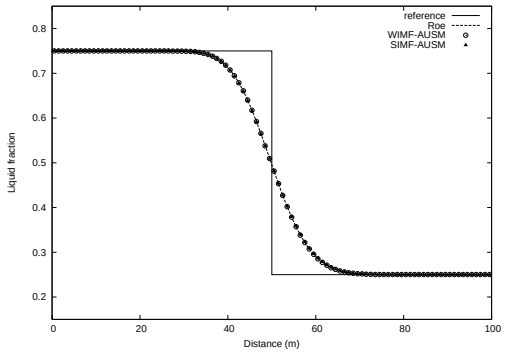

FIGURE 1. Linear contact discontinuity, 100 cells, T=5.0 s. Roe, SIMF-AUSM, and WIMF-AUSM scheme for $\Delta x/\Delta t = 1000$ m/s.

6. Numerical Simulations

In the first example we study the performance of WIMF-AUSM and SIMF-AUSM for a linear contact discontinuity. In particular,

- we want to demonstrate that WIMF-AUSM possesses the "exact resolution property" of Lemma 2 and is "weakly implicit" in the sense of Definition 4;
- we want to demonstrate that SIMF-AUSM is "strongly implicit" in the sense of Definition 5.

The purpose of the rest of the examples is to demonstrate that these "good" properties observed for WIMF-AUSM and SIMF-AUSM for a linear contact discontinuity to a large extent carry over to more difficult flow cases. For many flow cases we also include results produced by the explicit Roe scheme considered in [10].

6.1. **Linear Contact Dicontinuity.** We now wish to illustrate the properties of WIMF-AUSM and SIMF-AUSM as stated in Section 5. We consider a simple linear contact discontinuity in the volume fraction, where the initial states are given by

$$\mathbf{W}_{\mathrm{L}} = \begin{bmatrix} p \\ \alpha_{\mathrm{l}} \\ v_{\mathrm{g}} \\ v_{\mathrm{l}} \end{bmatrix} = \begin{bmatrix} 10^5 \text{ Pa} \\ 0.75 \\ 10 \text{ m/s} \\ 10 \text{ m/s} \end{bmatrix} \tag{83}$$

and

$$\mathbf{W}_{\mathrm{R}} = \begin{bmatrix} p \\ \alpha_{\mathrm{l}} \\ v_{\mathrm{g}} \\ v_{\mathrm{l}} \end{bmatrix} = \begin{bmatrix} 10^5 \text{ Pa} \\ 0.25 \\ 10 \text{ m/s} \\ 10 \text{ m/s} \end{bmatrix}. \tag{84}$$

We consider a 100 m long pipe and assume that the discontinuity is initially located at $x = 0$. We use a computational grid of 100 cells and simulate a time of $t = 5.0$ s. The discontinuity will then have moved to the center of the pipe, being located at $x = 50$ m.

First, in Figure 1 we have plotted the solutions produced by the Roe, WIMF-AUSM, and SIMF-AUSM scheme when the timestep corresponding to $\Delta x/\Delta t = 1000$ m/s is applied. All three schemes are mass coherent, i.e. they produce the same upwind type of mass fluxes, and for this time step the solutions are the same, practically speaking.

Results for different lower values of $\Delta x/\Delta t$ are given in Figure 2 for the WIMF and SIMF scheme. For these larger values of Δt the Roe scheme becomes unstable since it must obey the sonic CFL condition (2). SIMF-AUSM and WIMF-AUSM behave very similarly for a low timestep ($\Delta x/\Delta t = 1000$ m/s). However, increasing the timestep increases the accuracy for WIMF-AUSM but decreases it for SIMF-AUSM.

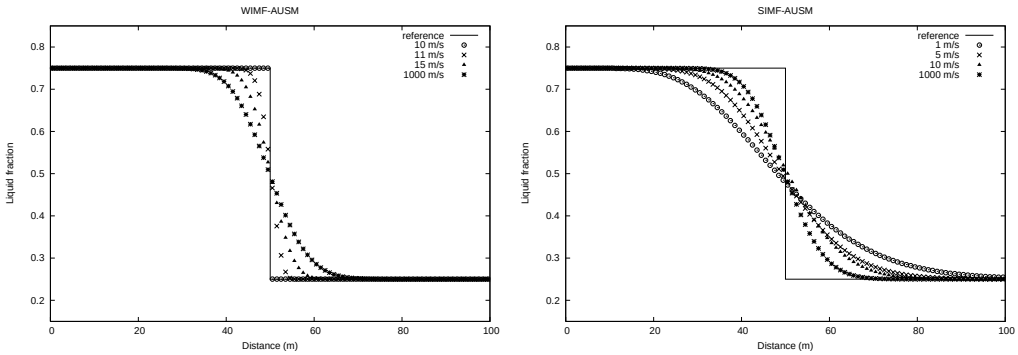

FIGURE 2. Linear contact discontinuity, 100 cells. SIMF-AUSM vs WIMF-AUSM scheme for different values of $\Delta x/\Delta t$. Left: WIMF-AUSM. Right: SIMF-AUSM.

We observe that for the critical timestep $\Delta x/\Delta t = v_{\mathrm{g}} = v_{\mathrm{l}} = 10$ m/s, WIMF-AUSM captures the discontinuity exactly, as stated by Lemma 2. Increasing the timestep beyond this value will make the WIMF-AUSM scheme unstable. On the other hand, we may increase the timestep beyond $\Delta x/\Delta t = 10$ m/s for SIMF-AUSM without inducing instabilities. Once we exceed this critical timestep, there is a significant increase in numerical diffusion.

Thus, we may conclude that the WIMF-AUSM scheme is *weakly implicit* in the sense of Definition 4 whereas the SIMF-AUSM scheme is *strongly implicit* in the sense of Definition 5. In addition, we have demonstrated that the WIMF-AUSM scheme possesses the "exact resolution property" of Lemma 2.

6.2. **Water Faucet Problem.** We now choose another problem which focuses on volume fraction waves. We consider the classical faucet flow problem of Ransom [20], which has become a standard benchmark [4, 10, 25, 18, 26].

We consider a vertical pipe of length 12 m with the initial uniform state

$$\mathbf{W} = \begin{bmatrix} p \\ \alpha_{\mathrm{l}} \\ v_{\mathrm{g}} \\ v_{\mathrm{l}} \end{bmatrix} = \begin{bmatrix} 10^5 \text{ Pa} \\ 0.8 \\ 0 \\ 10 \text{ m/s} \end{bmatrix}. \tag{85}$$

Gravity is the only source term taken into account, i.e. in the framework of (7) and (8) we have

$$Q_k = g\rho_k\alpha_k, \tag{86}$$

with g being the acceleration of gravity. At the inlet we have the constant conditions $\alpha_{\mathrm{l}} = 0.8$, $v_{\mathrm{l}} = 10$ m/s and $v_{\mathrm{g}} = 0$. At the outlet the pipe is open to the ambient pressure $p = 10^5$ Pa.

We restate the approximate analytical solution presented in the references [19, 26]

$$v_{\mathrm{l}}(x,t) = \begin{cases} \sqrt{v_0^2 + 2gx} & \text{for } x < v_0 t + \frac{1}{2}gt^2 \\ v_0 + gt & \text{otherwise.} \end{cases} \tag{87}$$

$$\alpha_{\mathrm{l}}(x,t) = \begin{cases} \alpha_0(1 + 2gxv_0^{-2})^{-1/2} & \text{for } x < v_0 t + \frac{1}{2}gt^2 \\ \alpha_0 & \text{otherwise} \end{cases} \tag{88}$$

where the parameters $\alpha_0 = 0.8$ and $v_0 = 10$ m/s are the initial states.

In Figure 3 we compare the SIMF-AUSM and the Roe scheme for $T = 0.6$ s on a grid of 120 computational cells. In addition, the effect of reducing the timestep to $\lambda = 17$ m/s is investigated for the SIMF-AUSM and the WIMF-AUSM scheme.

We note that for the small timestep $\lambda = 1000$ m/s the SIMF-AUSM scheme is virtually indistinguishable from the Roe scheme. Only for the pressure is any difference visible, here the SIMF-AUSM scheme is slightly more diffusive.

However, increasing the timestep to $\lambda = 17$ m/s (approximately the liquid velocity) causes a significant increase in numerical diffusion for the SIMF-AUSM scheme, both in pressure and

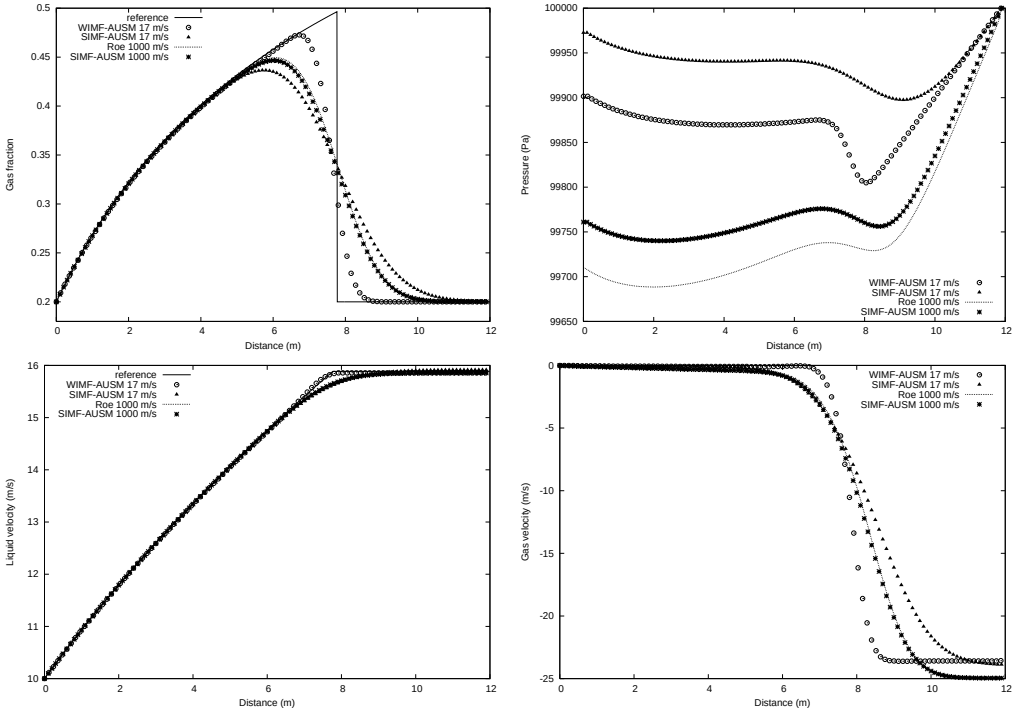

FIGURE 3. Water faucet problem, 120 cells, T=0.6 s. SIMF-AUSM, WIMF-AUSM and Roe scheme. Top left: Gas fraction. Top right: Pressure. Bottom left: Liquid velocity. Bottom right: Gas velocity.

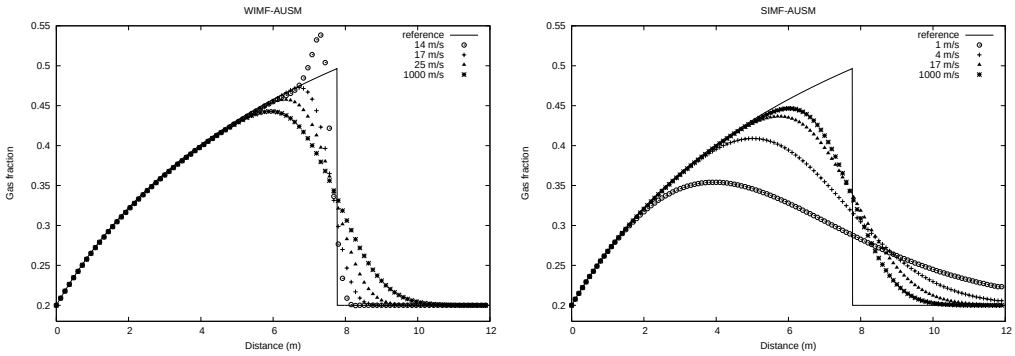

FIGURE 4. Water faucet problem, 120 cells. SIMF-AUSM vs WIMF-AUSM scheme for different values of $\Delta x/\Delta t$. Left: WIMF-AUSM. Right: SIMF-AUSM.

volume fraction. This sharply contrasts the results of the WIMF-AUSM scheme, where the lower integration velocity significantly improves the performance of the scheme on the slow waves.

6.2.1. *Effect of increasing the timestep.* We now investigate further how the SIMF and WIMF schemes behave under different timesteps. Results after $t = 0.6$ s are given in Figure 4.

We observe the same picture as for the linear contact discontinuity studied in the previous section. For low timesteps, the SIMF-AUSM and WIMF-AUSM have a similar behaviour. Increasing the timestep improves the accuracy of WIMF-AUSM but has the opposite effect on the SIMF scheme. Upon breaking the strong (volume fraction) CFL criterion, WIMF-AUSM becomes unstable whereas SIMF-AUSM merely becomes more diffusive.

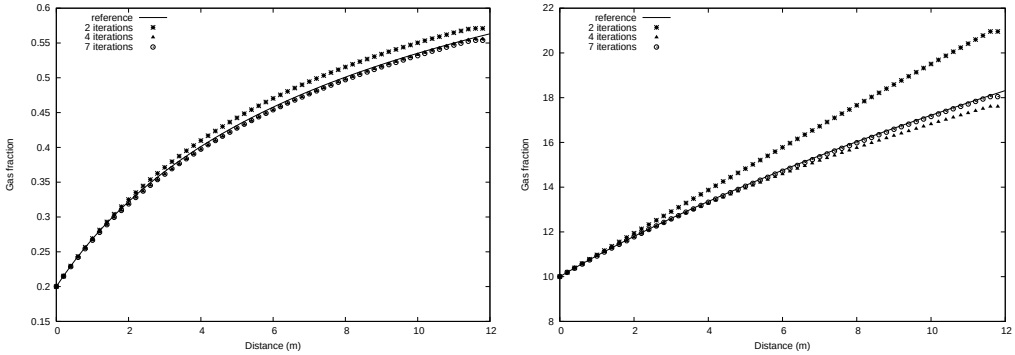

FIGURE 5. Water faucet problem, 60 cells, stationary conditions at T=5.0 s. SIMF-AUSM vs analytical solution. Left: Gas fraction. Right: Liquid velocity.

Remark 7. *These results confirm the picture observed in Section 6.1 and highlight an important difference between the SIMF and WIMF class of schemes. In effect, WIMF-AUSM reduces to the upwind explicit flux* (69) *for a contact discontinuity, whereas SIMF-AUSM reduces to the upwind implicit flux* (70).

6.2.2. *Stationary solution.* We now investigate the performance of the SIMF-AUSM scheme for very large timesteps, where the volume fraction CFL criterion is strongly violated.

Using the timestep $\Delta t = 5$ s, results after 2, 4 and 7 iterations are given in Figure 5, where the results are compared to the analytical stationary solutions. We observe that the SIMF-AUSM scheme produces qualitatively correct solutions already after 2 iterations. After 7 iterations, the numerical solutions coincide with the analytical reference solutions for liquid velocity and volume fraction.

6.3. **Toumi's Water-Air Shock.** We consider an initial value problem introduced by Toumi [24] and investigated by Tiselj and Petelin [23] and Paillère et al [19]. The initial states are given by

$$\mathbf{W}_{\mathrm{L}} = \begin{bmatrix} p \\ \alpha_{\mathrm{l}} \\ v_{\mathrm{g}} \\ v_{\mathrm{l}} \end{bmatrix} = \begin{bmatrix} 2 \cdot 10^7 \text{ Pa} \\ 0.75 \\ 0 \\ 0 \end{bmatrix} \tag{89}$$

and

$$\mathbf{W}_{\mathrm{R}} = \begin{bmatrix} p \\ \alpha_{\mathrm{l}} \\ v_{\mathrm{g}} \\ v_{\mathrm{l}} \end{bmatrix} = \begin{bmatrix} 1 \cdot 10^7 \text{ Pa} \\ 0.9 \\ 0 \\ 0 \end{bmatrix}. \tag{90}$$

No source terms are taken into account. For consistency with the work of Paillère et al [19], we modify the interfacial pressure correction (11) for this problem, setting $\sigma = 2$. Results after $T = 0.08$ s are given in figure 6, using a grid of 100 cells and a timestep $\Delta x/\Delta t = 1000$ m/s. Here we compare an explicit Roe scheme, the WIMF-AUSM scheme and the SIMF-AUSM scheme. The reference solution was calculated by the explicit MF-AUSMD scheme described in [12], using a grid of 10 000 cells.

We observe that the implicit schemes seem slightly more diffusive than the explicit Roe scheme. On the other hand, the Roe scheme seems to overshoot on the volume fraction waves compared to the reference solution.

We also note that for this low timestep, the SIMF-AUSM scheme and the WIMF-AUSM scheme produce virtually identical solutions.

6.3.1. *Effect of increasing the timestep.* We now consider the SIMF-AUSM scheme on a grid of 2000 cells for varying values of the integration parameter $\lambda = \Delta x/\Delta t$. Results for $\lambda = 1000$ m/s, $\lambda = 100$ m/s and $\lambda = 10$ m/s are given in Figure 7.

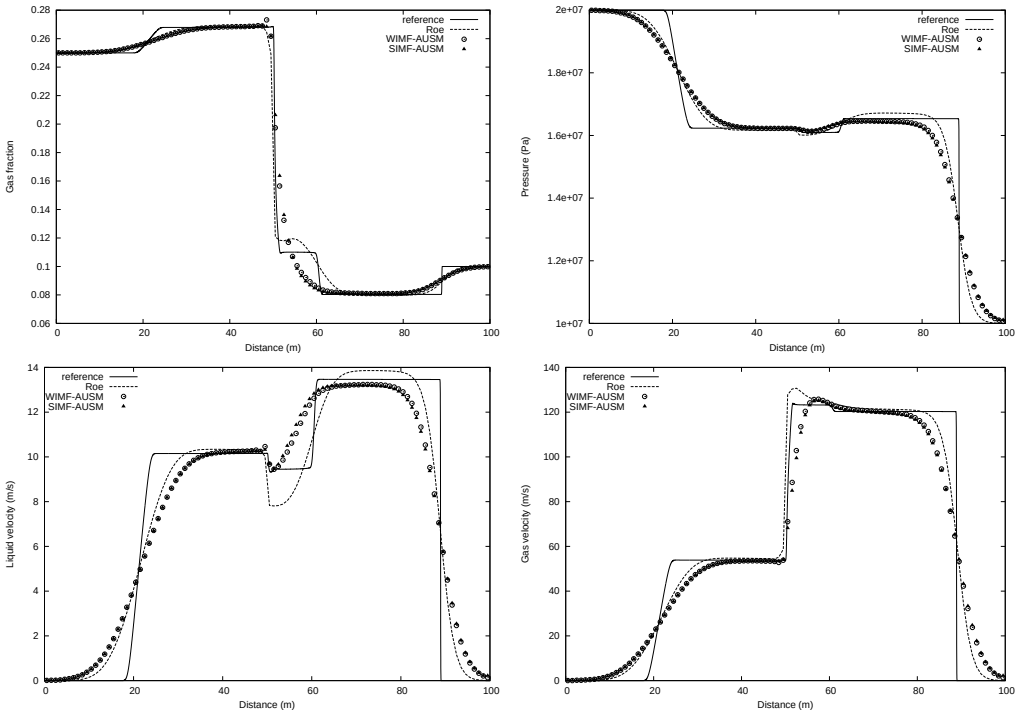

FIGURE 6. Toumi's shock tube problem, 100 cells. SIMF-AUSM, WIMF-AUSM and Roe scheme. Top left: Gas fraction. Top right: Pressure. Bottom left: Liquid velocity: Bottom right: Gas velocity.

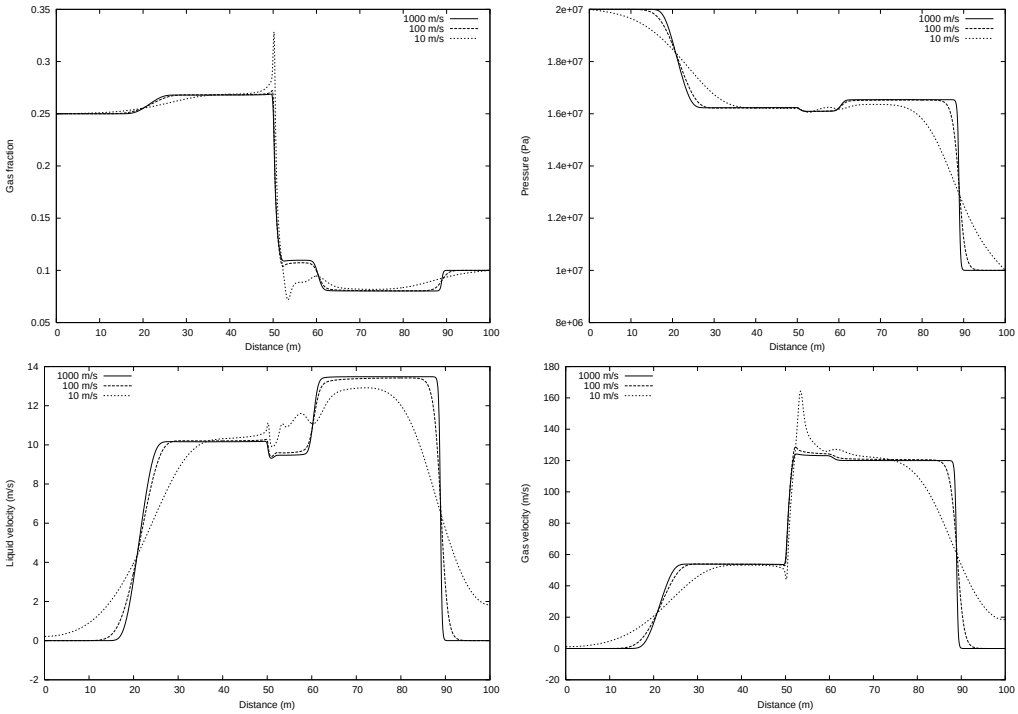

FIGURE 7. Toumi's shock tube problem, 2000 cells. Different timesteps for the SIMF-AUSM scheme. Top left: Liquid fraction. Top right: Pressure. Bottom left: Liquid velocity: Bottom right: Gas velocity.

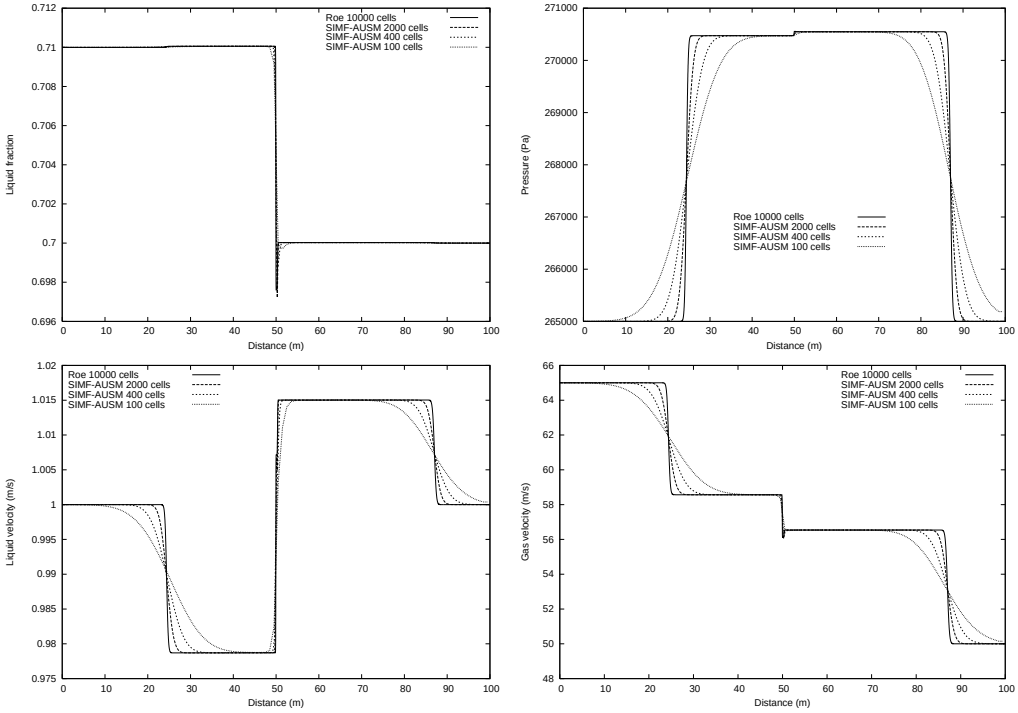

FIGURE 8. LRV shock tube problem. Grid refinement for the SIMF-AUSM scheme. Top left: Liquid fraction. Top right: Pressure. Bottom left: Liquid velocity: Bottom right: Gas velocity.

We observe that increasing the timestep to $\lambda = 100$ m/s has the effect of increasing the numerical diffusion on pressure waves. However, CFL instabilities are not produced even if the sonic CFL criterion is violated.

Increasing the timestep even further to $\lambda = 10$ m/s violates also the volume fraction CFL criterion. We note that the diffusion on the pressure waves is increased even further. CFL instabilities do not occur in the volume fraction waves, although for this high timestep spurious oscillations and overshoots are observed.

6.4. **A Large Relative Velocity Shock.** We consider the Riemann problem given by the initial states

$$\mathbf{W}_{\mathrm{L}} = \begin{bmatrix} p \\ \alpha_{\mathrm{l}} \\ v_{\mathrm{g}} \\ v_{\mathrm{l}} \end{bmatrix} = \begin{bmatrix} 265000 \text{ Pa} \\ 0.71 \\ 65 \text{ m/s} \\ 1 \text{ m/s} \end{bmatrix} \tag{91}$$

and

$$\mathbf{W}_{\mathrm{R}} = \begin{bmatrix} p \\ \alpha_{\mathrm{l}} \\ v_{\mathrm{g}} \\ v_{\mathrm{l}} \end{bmatrix} = \begin{bmatrix} 265000 \text{ Pa} \\ 0.7 \\ 50 \text{ m/s} \\ 1 \text{ m/s} \end{bmatrix}. \tag{92}$$

Again no source terms are taken into account. This initial value problem was proposed by Cortes et al [5] and is of interest in that the initial discontinuity contains a large difference in the relative velocity between the phases.

6.4.1. *Convergence of SIMF-AUSM scheme.* In Figure 8, grid refinement for the SIMF-AUSM scheme is studied using a timestep of $\lambda = 1000$ m/s. For reference, the Roe scheme on a grid of 10 000 cells is included. The simulation is carried out until the time $T = 0.1$ s is reached.

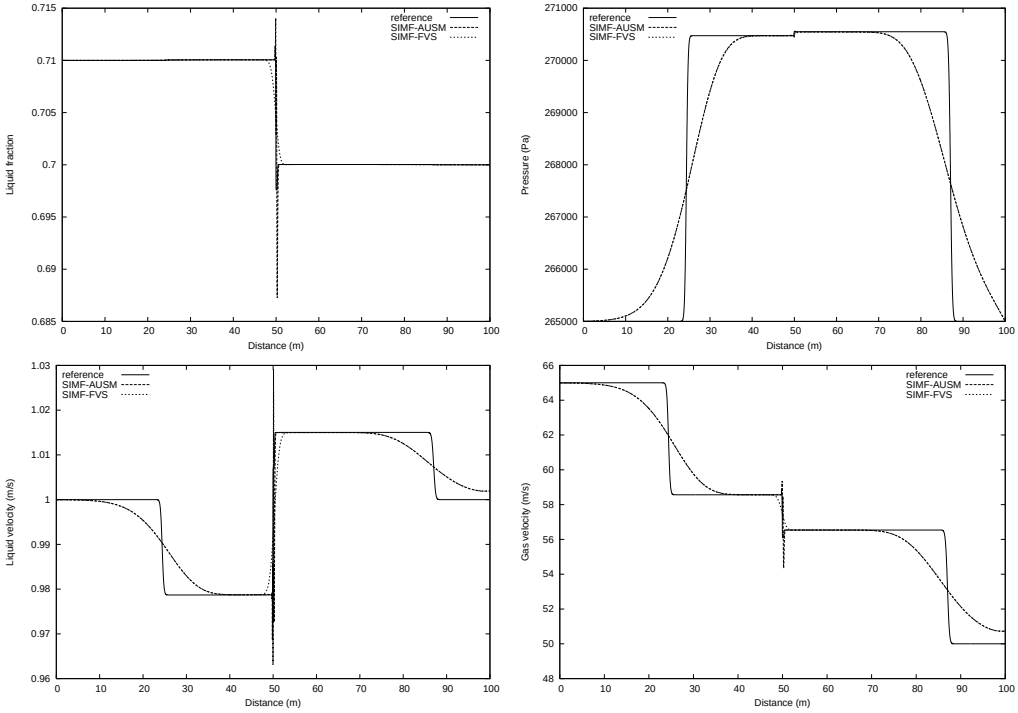

FIGURE 9. LRV shock tube problem, 2000 cells. Effect of large timestep for SIMF-AUSM and SIMF-FVS. Top left: Liquid fraction. Top right: Pressure. Bottom left: Liquid velocity: Bottom right: Gas velocity.

We see that the SIMF-AUSM scheme seems to converge to the reference Roe solution in a monotone way. Note that the wedge in the liquid fraction at $x = 50$ m is a slow moving wave structure, not a numerical oscillation.

6.4.2. *Comparison with SIMF-FVS scheme.* We now compare the SIMF-AUSM scheme with the SIMF-FVS scheme using a large timestep. We use a grid of 2000 cells and a timestep $\lambda = 10$ m/s, results are given in Figure 9.

We oberve that the schemes are indistuingishable on sonic waves. On volume fraction waves, the SIMF-AUSM scheme produces oscillations whereas the SIMF-FVS scheme is stable, yet somewhat diffusive.

Remark 8. *This is an interesting property of the SIMF-FVS scheme. Whereas the SIMF-AUSM is preferable for small timesteps due to its accuracy properties, the more diffusive SIMF-FVS has the ability of removing some stiffness from the system (58)–(61). Hence there may be cases where the SIMF-FVS is the preferable approach if large timesteps are used.*

6.5. **Separation Problem.** We follow Coquel et al [4] and consider a vertical pipe of length 7.5 m, where gravitational acceleration is the only source term taken into account. Initially the pipe is filled with stagnant liquid and gas with a uniform pressure of $p_0 = 10^5$ Pa and a uniform liquid fraction of $\alpha_1 = 0.5$. The pipe is considered to be closed at both ends, i.e. both phasic velocities are forced to be zero at the end points.

Assuming that the liquid column to be incompressible and freely falling under the influence of gravity, the following approximate analytical solution was derived [10] for the transient period

$$v_1(x,t) = \begin{cases} \sqrt{2gx} & \text{for } x < \frac{1}{2}gt^2 \\ gt & \text{for } \frac{1}{2}gt^2 \le x < L - \frac{1}{2}gt^2 \\ 0 & \text{for } L - \frac{1}{2}gt^2 < x \end{cases} \tag{93}$$

$$\alpha_{\rm l}(x,t) = \begin{cases} 0 & \text{for } x < \frac{1}{2}gt^2 \\ 0.5 & \text{for } \frac{1}{2}gt^2 \le x < L - \frac{1}{2}gt^2 \\ 1 & \text{for } L - \frac{1}{2}gt^2 < x \end{cases} \tag{94}$$

where $L = 7.5$ m is the length of the tube. This approximate solution consists of a contact discontinuity at the top of the tube and a shock-like discontinuity at the lower part of the tube. After the time

$$T = \sqrt{\frac{L}{g}} = 0.87 \text{ s} \tag{95}$$

these discontinuities will merge and the phases become fully separated. The volume fraction reach a stationary state, whereas the other variables slowly converge towards a stationary solution. In particular we expect the stationary pressure to be fully hydrostatic, approximately given by

$$p(x,t) = \begin{cases} p_0 & \text{for } x < L/2 \\ p_0 + \rho_{\rm l} g\,(x - L/2) & \text{for } x \ge L/2. \end{cases} \tag{96}$$

6.5.1. *Transition to one-phase flow.* As for the WIMF-AUSMD scheme [11], we observed that the basic SIMF-AUSM scheme could produce instabilities in the transition to one-phase flow.

Here we will follow a strategy successfully applied in earlier works [10, 11]. We consider a hybrid of the SIMF-AUSM and the SIMF-FVS scheme, denoted as SIMF-AUSM*, where the numerical convective fluxes $\mathbf{F} = (\rho\alpha v, \rho\alpha v^2)$ are given by the following expression

$$\mathbf{F}^{\text{SIMF-AUSM}^*} = s\mathbf{F}^{\text{SIMF-FVS}} + (1-s)\mathbf{F}^{\text{SIMF-AUSM}}. \tag{97}$$

Otherwise the SIMF-AUSM* scheme is identical to the SIMF-AUSM scheme. Here s is chosen as

$$s = \max(\phi_{\rm L}, \phi_{\rm R}), \tag{98}$$

where ϕ is an indicator function designed to be 1 near one-phase regions, 0 otherwise. For the purposes of this paper we follow [11] and choose

$$\phi_j = e^{-k_{\rm g}[\alpha_{\rm g}]_j^n} + e^{-k_{\rm l}[\alpha_{\rm l}]_j^n} \tag{99}$$

where we use the parameters $k_{\rm g} = 50$ and $k_{\rm l} = 500$.

We note that the SIMF-AUSM* scheme differs from the SIMF-AUSM scheme only near one-phase regions.

6.5.2. *Numerical results for the transient period.* In Figure 10 the results of the SIMF-AUSM* scheme are plotted for a grid of 100 cells and a timestep $\lambda = 100$ m/s. The simulation was carried out until the time $T = 0.6$ s was reached.

We observe good accordance with the expected analytical solutions.

6.5.3. *Numerical results for the stationary state.* Using the same grid of 100 cells and the timestep $\lambda = 100$ m/s, results for the SIMF-AUSM* scheme are plotted in Figure 11 at the time $T = 1.0$ s. Now quasi-stationary conditions are reached.

We see that the phases are well separated at this point. The lack of friction terms causes the gas velocity to be large as the gas phase is disappearing, which causes the pressure distribution to deviate slightly from the expected hydrostatic distribution.

6.5.4. *Convergence properties of SIMF-AUSM*.* In Figure 12 we investigate the convergence of the SIMF-AUSM* scheme as the grid is refined. We use the timestep $\lambda = 100$ m/s and the plot is made at the time $T = 0.6$ s. As we can see, the SIMF-AUSM* approximates the expected solution in a monotone way.

Remark 9. *An eigenvalue analysis* [10] *demonstrates that the volume fraction wave velocities are roughly given by*

$$\lambda^{\rm v} = \frac{\rho_{\rm g}\alpha_{\rm l}v_{\rm g} + \rho_{\rm l}\alpha_{\rm g}v_{\rm l}}{\rho_{\rm g}\alpha_{\rm l} + \rho_{\rm l}\alpha_{\rm g}} \pm \sqrt{\frac{\Delta p(\rho_{\rm g}\alpha_{\rm l} + \rho_{\rm l}\alpha_{\rm g}) - \rho_{\rm l}\rho_{\rm g}\alpha_{\rm l}\alpha_{\rm g}(v_{\rm g} - v_{\rm l})^2}{(\rho_{\rm g}\alpha_{\rm l} + \rho_{\rm l}\alpha_{\rm g})^2}}. \tag{100}$$

For this particular problem we see that these are approximately given by the gas velocity as the gas phase is disappearing. As the maximum gas velocity here becomes higher than the integration

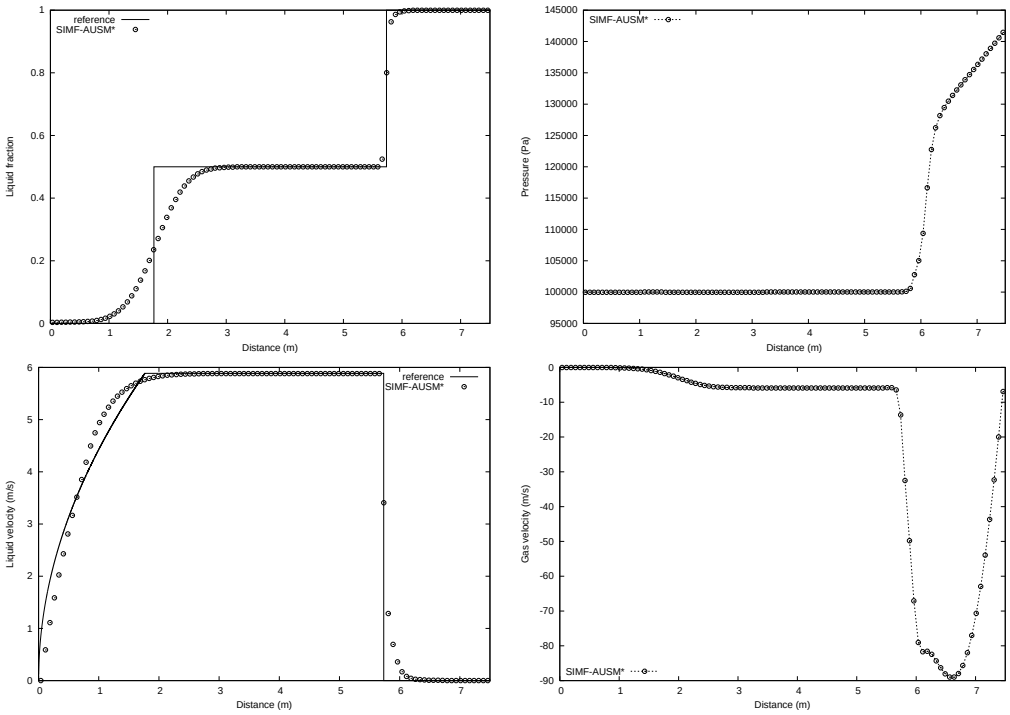

FIGURE 10. Separation problem, 100 cells. SIMF-AUSM* scheme at T=0.6 s. Top left: Liquid fraction. Top right: Pressure. Bottom left: Liquid velocity. Bottom right: Gas velocity.

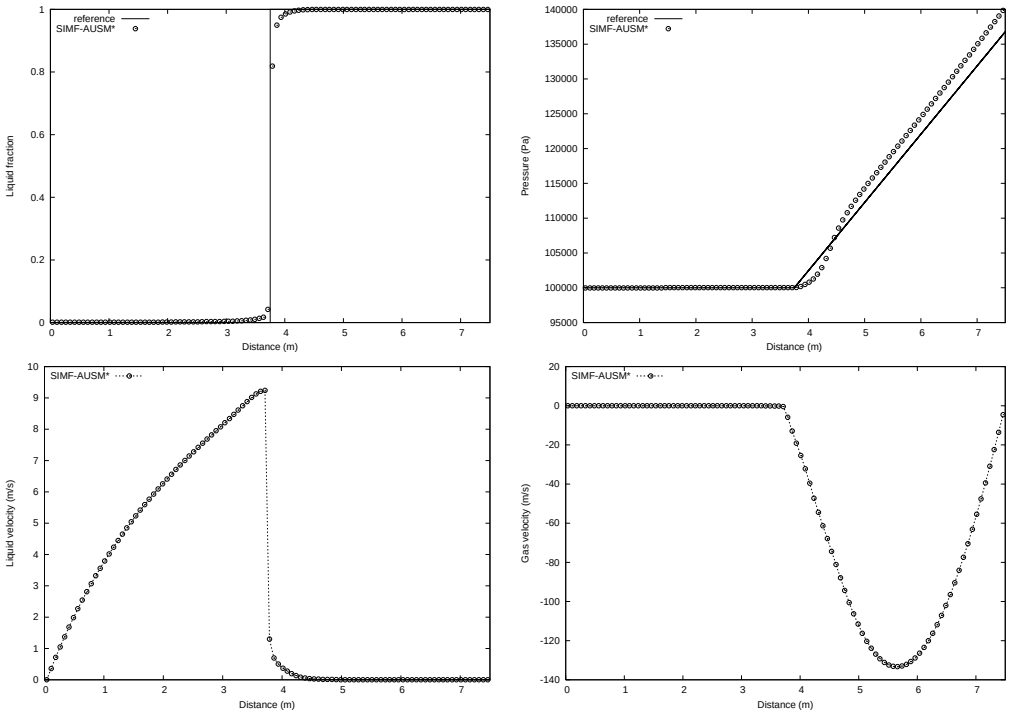

FIGURE 11. Separation problem, 100 cells. SIMF-AUSM* scheme at T=1.0 s. Top left: Liquid fraction. Top right: Pressure. Bottom left: Liquid velocity. Bottom right: Gas velocity.

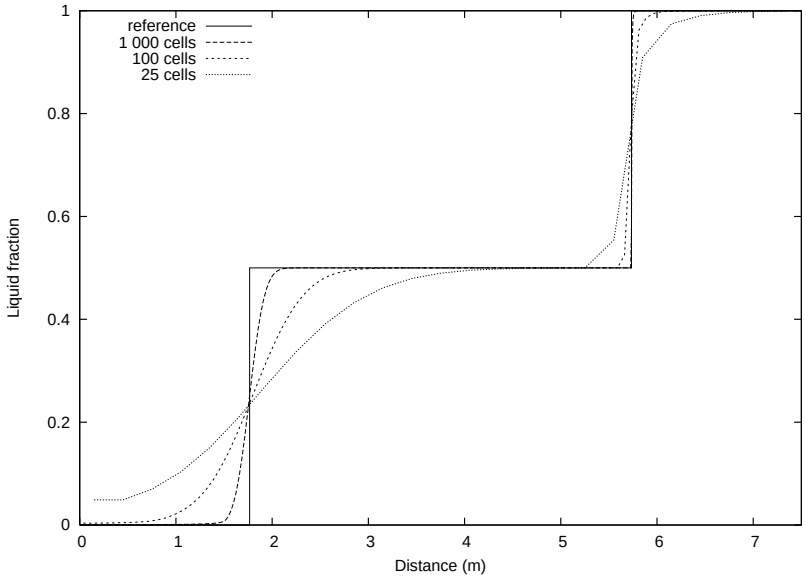

FIGURE 12. Separation problem, T=0.6s. Convergence properties of the SIMF-AUSM* scheme.

parameter λ, we conclude that the the SIMF-AUSM scheme is able to violate the CFL criterion for both sonic and volume fraction waves for this problem.*

6.6. **Oscillating Manometer Problem.** Finally, we consider a problem introduced by Ransom [20] and investigated in [19, 10, 11]. This problem tests the ability of numerical schemes to handle a change in the flow direction of a moving liquid plug.

We consider a U-shaped tube of total length 20 m. The geometry of the tube is reflected in the x-component of the gravity field

$$g_x(x) = \begin{cases} g & \text{for } 0 \le x \le 5 \text{ m} \\ g\cos\left(\frac{(x-5\text{ m})}{10\text{ m}}\pi\right) & \text{for } 5 \text{ m} < x \le 15 \text{ m} \\ -g & \text{for } 15 \text{ m} < x \le 20 \text{ m}. \end{cases} \tag{101}$$

Initally we assume that the liquid fraction is given by

$$\alpha_{\text{l}}(x) = \begin{cases} 10^{-6} & \text{for } 0 \le x \le 5 \text{ m} \\ 0.999 & \text{for } 5 \text{ m} < x \le 15 \text{ m} \\ 10^{-6} & \text{for } 15 \text{ m} < x \le 20 \text{ m}. \end{cases} \tag{102}$$

The initial pressure is assumed to be equal to the hydrostatic pressure distribution. We assume that the gas velocity is uniformly $v_{\text{g}} = 0$, and the liquid velocity distribution is given by

$$v_{\text{l}}(x) = \begin{cases} 0 & \text{for } 0 \le x \le 5 \text{ m} \\ V_0 & \text{for } 5 \text{ m} < x \le 15 \text{ m} \\ 0 & \text{for } 15 \text{ m} < x \le 20 \text{ m}, \end{cases} \tag{103}$$

where $V_0 = 2.1$ m/s.

Ransom [20] suggested treating the manometer as a closed loop. We will follow the approach of [19, 11], assuming that both ends of the manometer are open to the atmosphere. We assume that the liquid column will move with uniform velocity under the influence of gravity, giving the following approximate analytical solution for the liquid velocity [19]

$$v_{\text{l}}(t) = V_0 \cos(\omega t), \tag{104}$$

where

$$\omega = \sqrt{\frac{2g}{L}} \tag{105}$$

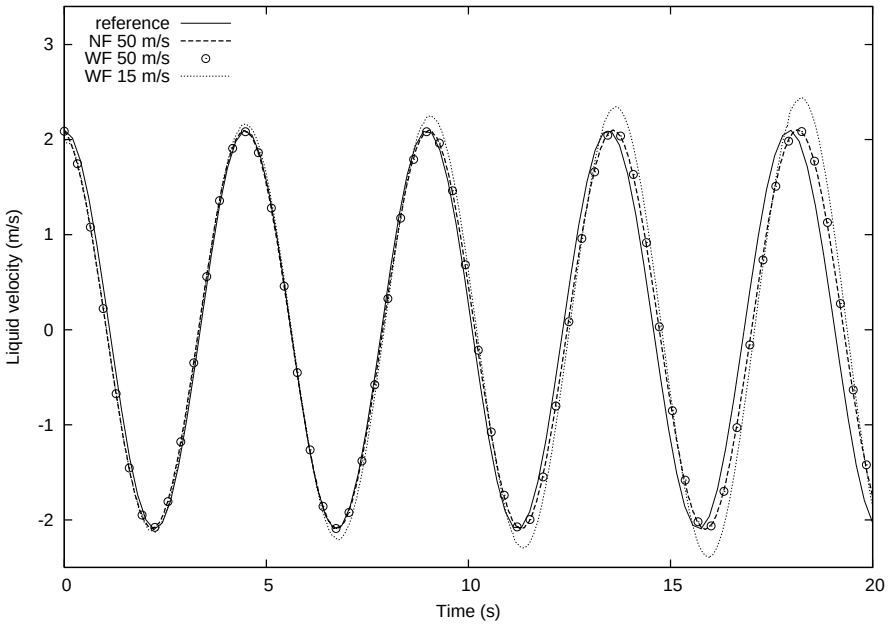

FIGURE 13. Oscillating manometer, 100 cells. SIMF-AUSM* scheme. Time development of the liquid velocity.

where $L = 10$ m is the length of the liquid column.

6.6.1. *Interfacial momentum exchange terms.* For this problem we will investigate the effect of including a source term modelling momentum exchange between the phases. For the gas momentum equation, we introduce the source term [19, 11]

$$M_{\mathrm{g}}^{\mathrm{D}} = C\alpha_{\mathrm{g}}\alpha_{\mathrm{l}}\rho_{\mathrm{g}}(v_{\mathrm{g}} - v_{\mathrm{l}}), \tag{106}$$

where C is a positive constant. Likewise the liquid momentum source term is given as

$$M_{\mathrm{l}}^{\mathrm{D}} = -M_{\mathrm{g}}^{\mathrm{D}} = -C\alpha_{\mathrm{g}}\alpha_{\mathrm{l}}\rho_{\mathrm{g}}(v_{\mathrm{g}} - v_{\mathrm{l}}), \tag{107}$$

conserving total momentum. We write

$$C = C_0\phi, \tag{108}$$

making the exchange term kick in more strongly near one-phase regions. For the purposes of this paper we choose

$$C_0 = 1000\ \mathrm{s}^{-1}, \tag{109}$$

and use a semi-implicit discretization as follows

$$(M_{\mathrm{g}}^{\mathrm{D}})_j^{n+1/2} = C_j^n(\alpha_{\mathrm{g}}\alpha_{\mathrm{l}}\rho_{\mathrm{g}})_j^n \left[\frac{(I_{\mathrm{g}})_j^{n+1}}{(m_{\mathrm{g}})_j^n} - \frac{(I_{\mathrm{l}})_j^{n+1}}{(m_{\mathrm{l}})_j^n}\right]. \tag{110}$$

We now consider the following models:

WF (With friction). We use the momentum exchange terms $M_{\mathrm{l}}^{\mathrm{D}}$ and $M_{\mathrm{g}}^{\mathrm{D}}$ as described above.
NF (No friction). We set $M_{\mathrm{l}}^{\mathrm{D}} = -M_{\mathrm{g}}^{\mathrm{D}} = 0$.

6.6.2. *Temporal evolution of the liquid velocity.* Using a grid of 100 cells, the evolution of the center cell liquid velocity is given in Figure 13. For the frictionless model the timestep $\Delta x/\Delta t = 50$ m/s was used. By including the friction terms, we found we could increase the timestep to $\Delta x/\Delta t = 15$ m/s without losing stability. However, for this timestep a non-physical increase in momentum is observed due to the coarse Euler discretization of the gravity field.

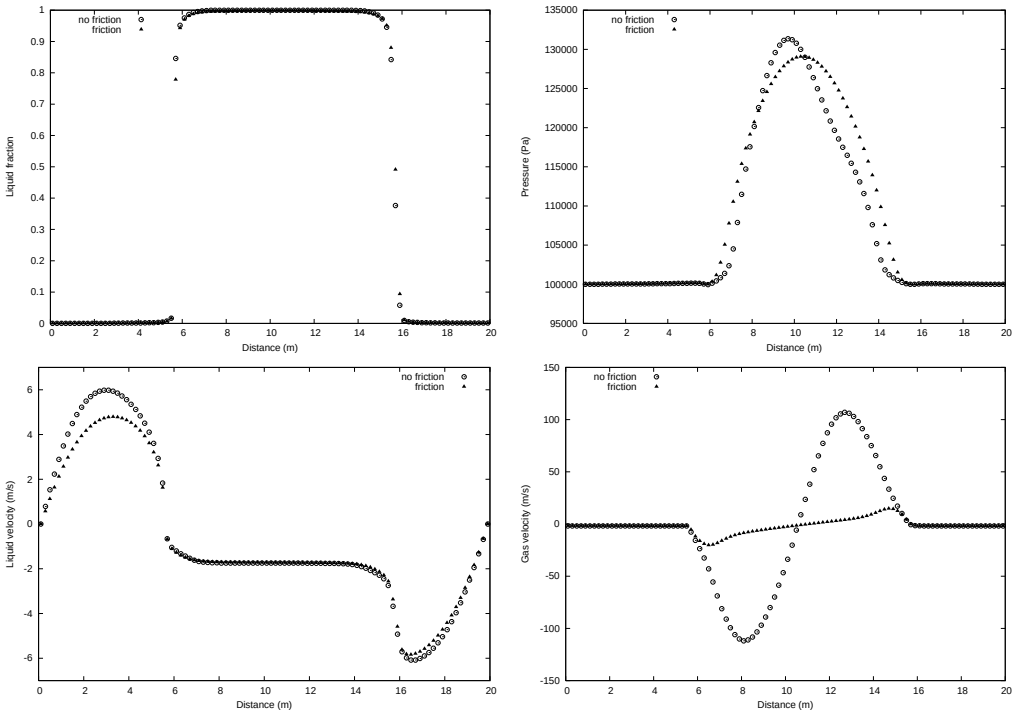

FIGURE 14. Oscillating manometer, t=20.0 s, 100 grid cells. SIMF-AUSM* scheme. Top left: Liquid fraction. Top right: Pressure. Bottom left: Liquid velocity. Bottom right: Gas velocity

We observe little difference between WF and NF for $\Delta x/\Delta t = 50$ m/s, where we achieve good accordance with the expected analytical solution. A slight phase difference seems to develop, which is in accordance with previous results [19, 10, 11].

6.6.3. *Frictionless versus frictional flow.* The distribution of all variables after $t = 20.0$ s is given in Figure 14 for the grid of 100 cells and the timestep $\Delta x/\Delta t = 50$ m/s.

We see that the inclusion of interfacial friction terms has the effect of reducing the gas velocity in the near one-phase liquid regions. As an effect of this, the pressure distribution approximates more accurately the expected hydrostatic distribution.

By the comments of Remark 9, we see that we are able to violate the CFL criterion for all waves also for this problem.

7. SUMMARY

We have constructed a framework termed *Strongly Implicit Mixture Flux* (SIMF) which allows us to construct fully CFL-free numerical schemes for a standard two-fluid model. This class of schemes keeps the accuracy and stability properties of its explicit predecessors for small timesteps.

Within this framework we have constructed natural extensions of the schemes investigated by Evje et al [8, 10, 12, 11], resulting in the WIMF-AUSM, SIMF-AUSM, and SIMF-FVS schemes.

We have demonstrated that the SIMF-AUSM scheme possesses accuracy and stability properties comparable to the Roe scheme for small timesteps. On breaking the sonic CFL criterion, the SIMF-AUSM scheme becomes less accurate than its weakly implicit variant WIMF-AUSM in the resolution of volume fraction waves.

Based on observations in this paper as well as previous works [12, 11], we may classify schemes in terms of their applicability as follows:

- *Explicit schemes.* Due to their easy and efficient implementation, explicit schemes are suitable for applications where fast pressure transients are of interest. This may more

often be the case for the nuclear industry than for the petroleum industry, where slow transients related to mass transport are generally more interesting.

- *Weakly implicit schemes.* These schemes are superior to explicit schemes in stability for large timesteps and accuracy on the slower waves. In particular, by choosing the timestep optimally, weakly implicit schemes may capture a moving contact discontinuity exactly. Consequently these schemes may be suitable for cases where slow transients are the main focus.
- *Strongly implicit schemes.* These schemes are superior to weakly implicit schemes in stability for very large timesteps. However, they are more diffusive and do not easily allow for high-resolution extensions like the MUSCL strategy of van Leer [14]. For this reason they are not well suited for cases where accurate tracking of the volume fraction waves is of interest. On the other hand, strongly implicit schemes may be used as steady state solvers or for cases where a computationally cheap qualitative description of the transient is desired.

Acknowledgements. The second author thanks the Norwegian Research Council for financial support through the "Petronics" programme.

References

[1] R. Abgrall, How to prevent pressure oscillations in multicomponent flow calculations, *J. Comput. Phys.* **125**, 150–160, 1996.
[2] F. Barre et al. The cathare code strategy and assessment, *Nucl. Eng. Des.* **124**, 257–284, 1990.
[3] K. H. Bendiksen, D. Malnes, R. Moe, and S. Nuland, The dynamic two-fluid model OLGA: Theory and application, in *SPE Prod. Eng.* **6**, 171–180, 1991.
[4] F.Coquel, K. El Amine, E. Godlewski, B. Perthame, and P. Rascle, A numerical method using upwind schemes for the resolution of two-phase flows, *J. Comput. Phys.* **136**, 272–288, 1997.
[5] J. Cortes, A. Debussche, and I. Toumi, A density perturbation method to study the eigenstructure of two-phase flow equation systems, *J. Comput. Phys.* **147**, 463–484, 1998.
[6] J. R. Edwards, R. K. Franklin, and M.-S. Liou, Low-diffusion flux-splitting methods for real fluid flows with phase transition, *AIAA Journal* **38**, 1624-1633, 2000.
[7] J. R. Edwards and M.-S. Liou, Low-diffusion flux-splitting methods for flows at all speeds, *AIAA Journal* **36**, 1610-1617, 1998.
[8] S. Evje and K. K. Fjelde, Hybrid flux-splitting schemes for a two-phase flow model, *J. Comput. Phys.* **175**, 674–701, 2002.
[9] S. Evje and K. K. Fjelde, On a rough ausm scheme for a one-dimensional two-phase flow model, *Comput. & Fluids* **32**, 1497–1530, 2003.
[10] S. Evje and T. Flatten. Hybrid flux-splitting schemes for a common two-fluid model. *J. Comput. Phys*, to appear.
[11] S. Evje and T. Flatten. Weakly implicit numerical schemes for the two-fluid model. Submitted for publication, August 2003.
[12] T. Flatten and S. Evje. A mixture flux approach for accurate resolution of two-phase flows. Submitted for publication, July 2003.
[13] M. Larsen, E. Hustvedt, P. Hedne, and T. Straume, Petra: A novel computer code for simulation of slug flow, in *SPE Annual Technical Conference and Exhibition*, SPE 38841, p. 1–12, October 1997.
[14] B. V. Leer, Towards the ultimate conservative difference scheme V. A second-order sequel to godunov's method, *J. Comput. Phys.* **32**, 101–136, 1979.
[15] M.-S. Liou, A sequel to AUSM: AUSM(+), *J. Comput. Phys.* **129**, 364–382, 1996.
[16] M.-S. Liou and C. J. Steffen, A new flux splitting scheme, *J. Comput. Phys.* **107**, 23-39, 1993.
[17] Y. Y. Niu, Simple conservative flux splitting for multi-component flow calculations, *Num. Heat Trans.* **38**, 203-222, 2000.
[18] Y.-Y. Niu, Advection upwinding splitting method to solve a compressible two-fluid model, *Int. J. Numer. Meth. Fluids* **36**, 351–371, 2001.
[19] H. Paillère, C. Corre and J.R.G Cascales, On the extension of the AUSM+ scheme to compressible two-fluid models, *Comput. & Fluids* **32**, 891–916, 2003.
[20] V. H. Ransom, Numerical bencmark tests, *Multiphase Sci. Tech.* **3**, 465-473, 1987.
[21] R. Saurel and R. Abgrall, A multiphase godunov method for compressible multifluid and multiphase flows, *J. Comput. Phys.* **150**, 425–467, 1999.
[22] R. Saurel and R. Abgrall, A simple method for compressible multifluid flows, *SIAM J. Sci. Comp.* **21**, 1115–1145, 1999.
[23] I. Tiselj and S. Petelin, Modelling of two-phase flow with second-order accurate scheme, *J. Comput. Phys.* **136**, 503–521, 1997.

[24] I. Toumi, An upwind numerical method for two-fluid two-phase flow models, *Nuc. Sci. Eng.* **123**, 147–168, 1996.

[25] I. Toumi and A. Kumbaro, An approximate linearized riemann solver for a two-fluid model, *J. Comput. Phys.* **124**, 286–300, 1996.

[26] J. A. Trapp and R. A. Riemke, A nearly-implicit hydrodynamic numerical scheme for two-phase flows, *J. Comput. Phys.* **66**, 62–82, 1986.

[27] Y. Wada and M.-S. Liou, An accurate and robust flux splitting scheme for shock and contact discontinuities, *SIAM J. Sci. Comput.* **18**, 633–657, 1997.